



HAL
open science

Design, Synthesis, and Evaluation of 2,9-Bis[(substituted-aminomethyl)phenyl]-1,10- phenanthroline Derivatives as G-Quadruplex Ligands.

Nassima Meriem Gueddouda, Rosales Myanou Hurtado, Stéphane Moreau, Luisa Ronga, Rabindra Nath Das, Solène Savrimoutou, Sandra Rubio, Adrien Marchand, Oscar Mendoza, Mathieu Marchivie, et al.

► To cite this version:

Nassima Meriem Gueddouda, Rosales Myanou Hurtado, Stéphane Moreau, Luisa Ronga, Rabindra Nath Das, et al.. Design, Synthesis, and Evaluation of 2,9-Bis[(substituted-aminomethyl)phenyl]-1,10-phenanthroline Derivatives as G-Quadruplex Ligands.. ChemMedChem, 2017, 12 (2), pp.146-160. 10.1002/cmdc.201600511 . hal-01461586

HAL Id: hal-01461586

<https://hal.science/hal-01461586>

Submitted on 12 Nov 2019

HAL is a multi-disciplinary open access archive for the deposit and dissemination of scientific research documents, whether they are published or not. The documents may come from teaching and research institutions in France or abroad, or from public or private research centers.

L'archive ouverte pluridisciplinaire **HAL**, est destinée au dépôt et à la diffusion de documents scientifiques de niveau recherche, publiés ou non, émanant des établissements d'enseignement et de recherche français ou étrangers, des laboratoires publics ou privés.

Design, synthesis, and evaluation of 2,9-bis[(substituted-aminomethyl)phenyl]-1,10-phenanthroline derivatives as G-quadruplex ligands

Nassima Meriem Gueddouda,^[a] Miyanou Rosales Hurtado,^[a] Stéphane Moreau,^[a] Luisa Ronga,^[a] Rabindra Nath Das,^[a] Solène Savrimoutou,^[a] Sandra Rubio,^[a] Adrien Marchand,^[a] Oscar Mendoza,^[a] Mathieu Marchivie,^[b] Lilian Elmi,^[a] Albain Chansavang,^[a] Vanessa Desplat,^[c] Valérie Gabelica,^[a] Anne Bourdoncle,^[a] Jean-Louis Mergny*^[a] and Jean Guillon*^[a]

- [a] Mrs. N. M. Gueddouda, Mrs. M. Rosales Hurtado, Dr. S. Moreau, Dr. L. Ronga, Dr. R. N. Das, Ms S. Savrimoutou, Dr. S. Rubio, Mr A. Marchand, Dr. O. Mendoza, Mr. L. Elmi, Mr. A. Chansavang, Dr. V. Gabelica, Dr. A. Bourdoncle, Dr. J.-L. Mergny and Pr. J. Guillon
Univ. Bordeaux, ARNA laboratory, CNRS UMR 5320, Inserm U1212, F-33076 Bordeaux, France
E-mail: jean-louis.mergny@inserm.fr
- [b] Dr. M. Marchivie
Univ. Bordeaux, ICMCB CNRS-UPR 9048, F- 33608 Pessac, France
- [c] Dr. V. Desplat
Univ. Bordeaux, UFR des Sciences Pharmaceutiques, Biothérapie des Maladies Génétiques Inflammatoires et Cancers, INSERM U1035, F-33076 Bordeaux cedex, France

Abstract:

Genomic sequences able to form guanine quadruplexes (G4) are found in oncogene promoters, in telomeres and in 5' and 3' untranslated regions as well as introns of messenger RNAs. These regions are potential targets for drugs designed to treat cancer. In the present work, we present the design and syntheses of ten new phenanthroline derivatives and characterization of their interactions with G4-forming oligonucleotides. We evaluated ligand-induced stabilization and specificity and selectivity of ligands for various G4 conformations using FRET-melting experiments. We investigated the interaction of compound **1a**, which combined the greatest stabilising effect and specificity for G4, with human telomeric sequences using FRET, circular dichroism and ESI-MS. In addition, we showed that compound **1a** interferes with the G4 helicase activity of *Saccharomyces cerevisiae* Pif1. Interestingly, compound **1a** was significantly more cytotoxic toward two human leukemic cell lines than to normal human blood mononuclear cells. These novel phenanthroline derivatives will be a starting point for further development and optimization of potent G4 ligands that have potential as anti-cancer agents.

Keywords

G-quadruplex; phenanthroline; G4 ligands; helicase assay; FRET-melting; circular dichroism.

Introduction

G-quadruplexes (G4) are secondary structures adopted by guanine-rich nucleic acids. G4 structures consist of a planar arrangement of two or more guanine quartets stabilized by cations (typically potassium or sodium) ^[1]. These structures have been detected in human cells using structure-specific antibodies ^[2,3], and computational studies have identified regions with the potential to form such structures in organisms such as the yeast *Saccharomyces cerevisiae* and human ^[4,5]. More than 370,000 sequences with potential to form G-quadruplex structures have been identified in the human genome ^[6,7]. Sequences prone to form G4 in human genome are found in key regions such as gene promoters, untranslated regions of messenger RNAs, telomeres, immunoglobulin switch regions, and in DNA replication origins ^[8]. Therefore, G-quadruplexes are likely involved in numerous biological processes such as transcription, translation, cell aging, and diseases such as cancer ^[9].

A number of proteins have been shown to interact with G-quadruplexes *in vitro* (for review ^[10]). Helicases such as Fanconi anaemia group J protein (Fanc J), Bloom syndrome protein (BLM), Werner syndrome protein (WRN), and Petite Integration Frequency 1 (PIF1) can unwind G4 structures formed by different sequences. Increases in cancer risk and/or genomic instability are associated with mutations that impair the function of these motor-like proteins ^[11].

Small molecules that specifically target G-quadruplexes have potential as anti-cancer drugs. It has been postulated that ligands that stabilize G-quadruplex structures will disturb or impede the expression of oncogenes containing one or more G4 motifs in their promoters. This hypothesis is supported by the fact that the potential to form G4 is higher in the promoters of oncogenes than in tumour suppressor genes ^[12]. Ligands that stabilize G-quadruplexes formed by the human telomeric DNA may also inhibit growth of cancer cells. Chromosomes end consist in 3' single-stranded TTAGGG repeats. These overhangs adopt G4 structures that inhibit telomerase activity *in vitro*. Telomerase, a reverse transcriptase that elongates telomeres, is overexpressed in most human cancers ^[13]. G4 stabilizing compounds may also promote telomere uncapping, which triggers the DNA damage response ^[14]. Both inhibition of telomere elongation and the DNA damage response can trigger a proliferation arrest resulting in anti-cancer activity.

Numerous G4 ligands belonging to different chemical families have been synthesized. Most of these ligands have scaffolds that consist of a planar aromatic core and chemical substituents that bear positive charges ^[15]. A large number of small heterocyclic molecules have been synthesized and evaluated for their ability to interact with G-quadruplexes ^[16]. Among them are the 1,10-phenanthroline derivatives, such as **PhenDC3** and its structural analogues **I**, tetra-amino-phenanthroline **II**, K35, and phenanthroline-2,9-bistriazole **III** (Figure 1) ^[17–28]. These compounds have been investigated for their capacity to bind and stabilize various G4 topologies and for their selectivity for G-quadruplex *versus* duplex structures.

The extended planar aromatic structure of the 1,10-phenanthroline scaffold provides a basis for efficient π - π stacking interactions with G-quartets. Here, we designed and synthesized ten new phenanthroline derivatives **1a-j**. We hypothesized that substitution with diaminobenzyl moieties in position 2 and 9 could lead to more potent G4 ligands in term of selectivity by increasing the aromatic surface and by enhancing aqueous solubility. This strategy has previously been reported for the design and synthesis of the disubstituted phenyl bis-oxazole **IV** (Figure 1) ^[29]. We reasoned that the extended aromatic structures of the diaminobenzyl groups would provide a basis for π - π stacking interactions with the G-quartets and that the length of the amine side chains could influence the stabilizing potential of the ligands. We evaluated ligand-induced stabilization, specificity, and selectivity of the newly synthesized phenanthroline derivatives for various G4 topologies through FRET-melting experiments. We further investigated the stoichiometries and the binding modes of the most potent derivatives with human telomeric sequences and determined the cytotoxicity against two different leukaemia cell lines and normal human peripheral blood mononuclear cells. Finally, we tested the ability of the ligands to interfere with the G4 unwinding activity of the Pif1 helicase from *S. cerevisiae*.

Results and Discussion

Chemistry

The reported 2,9-bis[(substituted-aminomethyl)phenyl]-1,10-phenanthroline derivatives **1a-i** were synthesized from the commercially available 2,9-dichloro-1,10-phenanthroline (Schemes 1 and 2). The bis-[2,9-(formylphenyl)]-1,10-phenanthrolines **2a-c** were easily prepared by a direct double-Suzuki-Miyaura cross-coupling reaction of 2,9-dichloro-1,10-phenanthroline with 2-, 3- or 4-formylphenylboronic acid performed in the presence of Pd(PPh₃)₄ as a catalyst, and in the presence of potassium (or sodium) carbonate as the base [30,31]. The structure of **2b** was established by X-ray crystallography, IR, and ¹H and ¹³C NMR data (Figure 2). Reaction of primary amines with **2a-c** gave the di-imines **3a-i**, which were reduced into the 2,9-bis[(substituted-aminomethyl)phenyl]-1,10-phenanthrolines **1a-i** using sodium borohydride in methanol as previously described [17]. The mono-substituted structural analogues of **1a-i** were obtained by substituting the 1,10-phenanthroline core with an aminomethyl)phenyl moiety substituted only at position 2. Using this singly substituted core, 2-{4-[(3-dimethylaminopropyl)aminomethyl]phenyl}-1,10-phenanthroline **1j** (Scheme 2) was obtained. The first attempts to synthesize the intermediate aldehyde **2d** by coupling 2-chloro-1,10-phenanthroline with 4-formylphenylboronic acid or 4-formylphenyl MIDA boronate failed. The mono-aldehyde **2d** was prepared using 4-formylphenylboronic acid pinacol ester under mild conditions in the presence of Pd(PPh₃)₄ and cesium carbonate as previously described [32]. Condensation of 3-(dimethylamino)-1-propylamine with aldehyde **2d** led to the imine **3j**, which was then converted to the 2-{4-[(3-dimethylaminopropyl)aminomethyl]phenyl}-1,10-phenanthroline **1j** by reduction with NaBH₄ as described above. These phenanthroline compounds **1a-j** were then converted into their ammonium oxalate salts by treatment with oxalic acid in refluxing isopropanol. Table 1 summarizes the physical properties of the **1a-j** oxalates.

Screening assays

To evaluate the ability of the synthesized compounds to interact with G4, we used three different FRET-melting experiments to determine; (i) ligand (**1a-j**) induced stabilization of a given G4 sequence, (ii) preferences for G4 over duplex, and (iii) specificity towards a particular G4 sequence. We first assessed the effect of increasing concentrations of ligands **1a-j** on the thermal stability of the G4 conformation adopted by the F21T DNA oligonucleotide (Supplementary Table 1), derived from the human telomere sequence, in K⁺ and in Na⁺ conditions. G4-forming oligonucleotides adopt various topologies *in vitro* depending on the length and sequence composition, the ionic environment, and the sample preparation. In K⁺, F21T adopts a mixture of G4 conformations containing an antiparallel and a 3+1 hybrid type topologies; in Na⁺ conditions, F21T forms an antiparallel G4 conformation. Each of the synthesized compounds **1a-j** stabilized F21T in both K⁺ (10 mM supplemented with 90 mM LiCl) and Na⁺ (100 mM) conditions, although to different extents (Supplementary Figure S1). This stabilization ($\Delta T_{1/2}$) was calculated from comparison of temperature of half denaturation ($T_{1/2}$) of the fluorescently labelled oligonucleotide in the presence or absence of the ligand. The well-characterized G-quadruplex ligand phenanthroline **PhenDC3** [17] (Figure 1) was used in these tests as a positive control. Our results showed that ligands **1a-j** were more stabilizing in K⁺ conditions than in Na⁺ conditions, and two ligands (compounds **1a** and **1b**) induced the highest increase in F21T thermal stability in both conditions (Figure 3 and Table 2). The least stabilizing compounds were derivatives **1h**, **1i**, and **1j**.

As these new tested ligands **1a-j** share the same phenanthroline core and differ in the nature and the position of the polyaminoalkyl chain substitutions, we tried to infer information on the structure-activity relationship (SAR) of these new synthetic compounds. The phenanthrolines **1a-d**, which are disubstituted with polyaminoalkyl chains on position 4 of the benzyl moieties, effectively stabilized the F21T structure. The $\Delta T_{1/2}$ ranged from 10.4 to 14.9 °C for the 4-substituted phenyl compounds **1a-d**, and the $\Delta T_{1/2}$ of phenanthrolines **1e-g** substituted in position 3 of the phenyl moieties ranged from 9.4 to 11.6 °C. When the benzyl moieties were modified with aminoalkyl chains on position 2 (compounds **1h** and **1i**), $\Delta T_{1/2}$ values ranged from 5.3 to 7.7 °C. Interestingly, in terms of average values, ligands bearing a methylpiperazine moiety on the aminoalkyl side chains of the benzyl could be generally considered slightly more efficient

stabilizers of F21T than the corresponding dimethylamino, pyrrolidine, or morpholine analogues in each subseries substituted on positions 2, 3, or 4. For example, compound **1b** stabilized F21T better than structural analogues **1c** or **1d** in the 4-substituted position. In the subseries in which the polyaminoalkyl side chain was anchored in position 3 of the benzyl ring, the piperazine substituted phenanthroline **1f** seemed to be slightly more stabilizing than derivatives **1e** and **1g**. The same observation could be found for substitution in position 2: $\Delta T_{1/2}$ was 5.3 °C for compound **1h** versus 7.7 °C for **1i**. Moreover, the mono-substitution of the phenanthroline core with a polyaminoalkylbenzyl substituent (compound **1j**) led to a decrease in the G4 stabilization ($\Delta T_{1/2} = 5.9$ °C) in comparison with its disubstituted analogue **1a** ($\Delta T_{1/2} = 14.0$ °C). Finally, compounds **1a-j** were found to be less effective F21T stabilizers than reference compound **PhenDC3**: *i.e.*, the $\Delta T_{1/2}$ for **PhenDC3** was noticed at 21.8 °C whereas $\Delta T_{1/2}$ values for phenanthrolines **1a-j** ranged from 5.3 to 14.9 °C.

To assess the ligand selectivity for G4, we performed a FRET-melting experiment in the presence of a self-complementary double-stranded DNA competitor ds26 (⁵d-CAATCGGATCGAATTCCGATCCGATTG³). For this experiment, we excluded compounds **1h**, **1i**, and **1j** as these ligands resulted in less than 10 °C of F21T stabilization in K⁺ conditions. We monitored F21T melting in the presence of 1 μM compounds **1a-g** and of an excess of ds26 as competitor (15 or 50 equivalents compared to F21T). No significant effect was observed for F21T thermal stability after addition of a 15 equivalent excess of competitor (3 μM) in the presence of the ligands tested, except for **1b** (Figure 4 and Table 2). Higher ds26 concentrations (15 μM - 50 equivalent excess) led to a decrease in ΔT_m for compounds **1b** and **1f**. In contrast, ds26 had no impact on the stabilizing effects of **1c** and **1e** and only marginally affected the stabilizing abilities of **1a**, **1d**, and **1g**.

The slight decrease in F21T thermal stability obtained in the presence of a large excess of ds26 reflects a fair selectivity towards the G4 structure. To confirm this observation we performed circular dichroism (CD) melting experiments. CD melting analysis showed that **1a** stabilised both 22AG and c-myc (unlabelled; Supplementary Table 2), but had little or no effect on ds26 melting temperature.

We estimated an index of selectivity *S* for each compound by calculating the ratio of F21T $\Delta T_{1/2}$ in the presence of ligand with 3 μM ds26 and F21T $\Delta T_{1/2}$ in the presence of ligand without competitor. Our results showed that all derivatives displayed selectivity toward F21T in K⁺ conditions with *S* between 0.82 and 0.93 (Table 2). When the stabilization ability and the selectivity index criteria were considered, compound **1a** was the most promising G4 ligand in this newly synthesized series.

To determine whether this promising phenanthroline **1a** could stabilize other G4-forming sequences, we performed FRET-melting assays with G-rich DNA oligonucleotides (Supplementary Table 1) that are known to adopt various G4 topologies [40] including parallel-stranded G4s such as F25cebT, derived from the human minisatellite sequence [41], and FcmycT, derived from a human oncogene promotor [42]; and anti-parallel G4s with two G-quartets such as FtbaT the thrombin binding aptamer sequence [43], and Fbom17T, a sequence derived from the *Bombyx mori* telomeres [44]. We also used F21RT, an RNA oligonucleotide derived from the human telomere sequence, which folds into a parallel G4, and FctaT, a DNA oligonucleotide which is a mutant variant derived from the DNA human telomeric sequence that adopts an anti-parallel G4 conformation [45]. Finally, we used the DNA oligonucleotide FdxT, a non-G4-forming control sequence, which folds onto an intramolecular duplex. For technical reasons, we used the same salt conditions for all the sequences tested (K⁺ conditions) with the exception of the F21RT. The potassium concentration for analysis of F21RT was 1 mM instead of 10 mM: at a 10 mM potassium concentration, the thermal stability of the G4 adopted by F21RT is too high to allow the measurement of the stabilization induced by a given ligand. Since G-quadruplex stability is cation concentration dependent, decreasing the potassium concentration enabled us to follow the ligand effect on this RNA sequence [46]. As shown in Figure 5, ligand **1a** preferentially stabilized the RNA (F21RT) and DNA (F21T) human telomeric sequences. Phenanthroline **1a** stabilized the mutated variant of the telomeric sequence (FctaT), the telomeric sequence from *B. mori* (Fbom17T), and the thrombin binding aptamer sequence (FtbaT) to a lesser extent than it did F21T. Compound **1a** did not stabilize the parallel DNA G4 structures adopted by F25cebT and FcmycT. These G4 forming sequences both possess three propeller loops (including a very long one for F25cebT).

Interestingly, the CD melting experiments showed greater stabilization of unlabelled cmyc oligonucleotide than did the FRET-melting experiments (Supplementary Table 2). Two factors may explain this apparent discrepancy: i) different oligonucleotides are used for these experiments: in FRET-melting we used a dual-labelled c-myc sequence while in CD we used unlabeled c-myc oligonucleotide; ii) oligonucleotide and compound concentrations are different, due to different sensitivities of the techniques. This observation also points out the necessity of performing complementary experiments using unlabelled sequences in addition to the FRET-melting screening assay. All of our results, however, suggest that compound **1a** preferentially stabilizes G4 structure adopted by the human telomeric sequences F21T and F21RT relative to those conformations adopted by the other oligonucleotides tested.

PhenDC3 has better G4 *versus* duplex selectivity than does **1a** (Table 2). In contrast, the FRET-melting assay showed that **1a** only preferentially stabilized the human telomeric sequences which suggests a better target specificity. Other G4 ligands, such as 360A and pyridostatin, interact differently with the same panel of oligonucleotides [40]. This finding emphasizes that the combination of different structural elements are critical for G4-ligand interactions resulting in various degrees of selectivity and specificity even for ligands that belong to the same chemical family.

Interaction mode investigation

Taken together, the FRET-melting results showed that of the newly synthesized ligands, **1a** displayed the best stabilization and showed a preference for the human telomeric sequences with an excellent G4 vs. duplex selectivity. Since human telomeric sequences can adopt different G-quadruplex conformations depending on their length and flanking bases [37], we performed CD titration experiments using the **1a** ligand with two different unlabelled sequences: 22AG and 24TTG (Supplementary Table 1). These oligonucleotides are 22 and 24 bases long, respectively.

The obtained CD spectra collected under identical K⁺ conditions showed first that 22AG and 24TTG sequences have different CD signatures. The CD spectrum of 22AG (3 μM) in absence of ligand has two positive peaks around 250 nm and 290 nm and a positive shoulder around 275 nm (Figure 6a, solid black line). The spectrum of 24TTG (3 μM) was characterized by higher amplitude peaks than observed in the spectrum of 22AG. The spectrum of 24TTG had a negative peak around 240 nm and two positive peaks around 270 and 290 nm (Figure 6b, solid black line). Upon addition of 1 to 5 equivalents of **1a** to the DNA, we observed the emergence of a positive peak between 260 and 265 nm in CD signatures of both oligonucleotides. In the case of 22AG, we observed a decrease in amplitude of the positive peaks at 290 nm and 250 nm and the appearance of a negative peak around 240 nm upon the addition of **1a** (Figure 6a, dashed lines). For 24TTG, a decrease in the amplitude of the positive peak at 290 nm was observed in the presence of **1a** (Figure 6a and 6b, dashed lines). In contrast, upon **PhenDC3** addition to 24TTG, we observed significant changes, with a decrease in the amplitudes of the positive peak at 270 nm and the negative peak around 240 nm and the appearance of two new peaks, one negative peak at 265 nm and one positive peak at 250 nm (Supplementary Figure S2).

PhenDC3 and **1a** also induced different changes in the CD profile of the mutated variant of the human telomeric sequence 22CTA. Upon the addition of **PhenDC3**, 22CTA kept its antiparallel conformation as demonstrated by increased amplitudes of the positive peak around 295 nm and the negative peak around 270 nm (Supplementary Figure S3b). In contrast, upon the addition of **1a** we observed the emergence of a new positive peak between 260 and 265 nm and a decrease in the amplitude of the positive peak around 295 nm. Further, the positive peak at 250 nm disappeared upon addition of **1a** and a new negative peak at 245 nm was observed. These results suggest that **1a** induces a change in the conformation of a significant fraction of 22CTA to a parallel G4 (Supplementary Figure S3a). This is one of the rare examples of ligand characterized that induces a change to the parallel conformation for the human telomeric G4 forming sequence. [39,47,48,58]

After confirming the interaction of **1a** with human DNA telomeric G4 forming sequences using CD, we performed titrations by mass spectrometry to better characterize this interaction [49]. Our first goal was

to determine the stoichiometry of interaction between **1a** and human DNA telomeric sequence. The second objective was to determine whether this interaction caused potassium displacement. This cation plays a pivotal role in G4 folding. One potassium ion can specifically intercalate between two G-quartet planes inside the G-quadruplex structure^[49]. Mass spectrometry has been used to determine whether the G4 interaction with a given ligand results in displacement of one or more potassium ions^[47]. We performed ESI-MS experiments with 10 μ M of 24TTG, which adopts a single G4 conformation in K⁺. 24TTG forms a 3+1 hybrid conformation containing three guanine quartets, which means that two potassium ions are bound by this oligonucleotide. A titration revealed that the stoichiometry of the interaction between **1a** and 24TTG is 2:1 (the 3:1 complex was completely absent) and that this interaction did not result in potassium displacement (Figure 7). In contrast, **PhenDC3** binding resulted in displacement of one potassium ion, and the major peak observed correspond to a complex containing one ligand and one oligonucleotide^[47].

Our results with **1a** and the human telomeric sequence 24TTG are consistent with the interaction of two ligands with each of the terminal G-quartets of a single G-quadruplex structure through π - π stacking as well as electrostatic interactions with the phosphate backbone. To confirm this hypothesis we performed molecular docking calculations using **1a** and three different G4 scaffolds based on the crystal structures of (i) the parallel conformation of 22AG(1KF1)^[50], (ii) the antiparallel conformation of 22CTA (2KM3)^[59] and (iii) the hybrid conformation of 24TTG (2GKU)^[60]. Indeed, we showed that **1a** induced changes in CD signature of 22AG, 24TTG and 22CTA DNA telomeric sequences in K⁺ conditions that suggest a transition to a parallel conformation (Figure 6, Figure S3a) and that **1a** significantly stabilized the parallel conformation adopted by F21RT (Figure 5). We docked then **1a** with these three different G4 forming sequences, and the most favourable complex for each scaffold based on the calculated binding energy was selected (Supplementary Figure S4). For the parallel oligonucleotide 1KF1, the phenanthroline moiety of ligand **1a** stacks on top of the G-quadruplex tetrad, which is consistent with π - π stacking interactions between **1a** and a G-quartet. The positively charged amine side chains were directed towards the negatively charged phosphate backbones of the oligonucleotides which facilitated the electrostatic interactions required for the stabilization. The ligand **1a** interacted with the antiparallel 22CTA (2KM3) and hybrid oligonucleotide 24TTG (2GKU) in a similar manner (Supplementary Figure S5, S6) and induced the parallel conformation which is in consistent with the CD results. As observed from the ESI-MS experiments, it is expected that another ligand molecule would bind at the opposite end of the quadruplex with the same mode of action.

Helicase inhibition

The aim of screening small molecules targeting G-quadruplex structures is to find strong G4 stabilizers in order to impede key biological processes. We tested the ability of **1a** to inhibit G-quadruplex unwinding by the *Saccharomyces cerevisiae* Pif1 helicase^[51]. This protein can unwind G-quadruplexes in an ATP-driven process in the presence of magnesium. This helicase is involved in DNA replication and in telomerase removal from telomeric DNA^[52,53]. We used the experimental conditions previously described^[54] to compare Pif1 activity on non-G4 containing systems and G4-containing systems (Supplementary Scheme 1). In the present work, we used two non-G4 systems as controls: *S-mut* in which the G4 region has been replaced with sequence unable to adopt a G4 fold and *S-dx*, in which the G4 region has been replaced with a region that forms a duplex. As we experienced reproducibility issues with the opening of the human telomeric G-quadruplexes, we chose to analyse the ability of **1a** to interfere with the helicase activity of Pif1 on *cmcy*, *25ceb*, and *TBA* G-quadruplexes. Our results showed that **1a** did not interfere with the helicase activity of Pif1 on single-stranded *S-mut* or the duplex-forming *S-dx* which confirm its G4 selectivity. In contrast, **1a** dramatically impeded the resolution of G4 in the *cmcy* and the *25ceb* systems (Figure 8). For *tba*, the presence of the ligand slightly inhibited unwinding by Pif1 (Figure 8). Our helicase assays also indicate that the ability of **1a** to inhibit Pif1 helicase activity towards a given target is not directly correlated with **1a** ability to stabilize the corresponding quadruplex in FRET-melting experiments. In contrast, in the same conditions **PhenDC3** inhibits the helicase activity of Pif1 toward all the tested G4-containing systems^[54]. Taken together, our results are in line with a better target specificity of **1a** when compared to **PhenDC3**.

Cytotoxic effects on human cells

We then tested for antiproliferative activity of ligands **1a** and **1b** against two human myeloid leukaemia cell line cultures. Against the human myeloid leukaemia cell line K562, phenanthrolines **1a** and **1b** showed antiproliferative activity with IC_{50} of 10 ± 0.2 and 9 ± 0.1 μ M, respectively. Compound **1a** also inhibited growth of HL60 human acute promyeloid leukemia cell line with an IC_{50} value of 11 ± 0.2 μ M. In addition, compounds **1a** and **1b** were tested on activated (PBMNC + PHA) human peripheral blood mononuclear cells to evaluate their cytotoxicity on normal cells. These two derivatives **1a-b** presented an IC_{50} superior to 50 μ M against lymphocytes. Indexes of selectivity (IS), defined as the ratio of the IC_{50} value against the human mononuclear cells to the IC_{50} values against the leukaemia lines, were greater than 4.5 for both the HL60 and the K562 cell lines.

Conclusion

We designed and synthesized ten new phenanthroline derivatives bearing polyaminoalkylbenzyl moieties in position 2 and/or 9. All these compounds stabilized the G-quadruplex structure formed by the fluorescently labelled human telomeric DNA sequence F21T. Most of the synthesized ligands displayed good selectivity for this G4 compared to duplex structures. We chose to study the interaction mode of the human telomeric DNA sequences with the promising G4 phenanthroline **1a** in more detail, as **1a** was the most potent ligand in terms of stabilization ability and selectivity. We confirmed that **1a** interacted with oligonucleotides not labelled with dyes, inducing their stabilization and impacting their CD signatures. Indeed, **1a** interact with DNA and RNA telomeric sequences (F21RT, 22AG, 24TTG, and 22CTA). Our data indicate that compound **1a** significantly stabilizes and/or induces a change to a parallel-like conformation upon binding. ESI-MS analyses revealed a 2:1 stoichiometry of interaction between **1a** and its G4 target. This result and our molecular docking experiments are consistent with a π - π stacking interaction mode between ligand and each terminal G-quartet. Finally, we also demonstrated that our ligand interfered with the unwinding of the G4 structures by the Pif1 helicase. Although **1a** and **PhenDC3** share a common phenanthroline core, our results shown that the two ligands interact differently with G4 structures. In particular, PhenDC3 binding to telomeric sequences is accompanied by cation ejection and induction of an antiparallel-type CD signature, whereas **1a** binding to telomeric G-quadruplexes induces a more parallel-type CD signature and does not cause potassium ion ejection. It will be interesting to investigate the *in vivo* effects of ligand **1a** as its properties *in vitro* suggest that it has potential in anti-cancer applications. Moreover, by taking into account the preliminary results and the structure-activity relationships of this new series, our data are a promising starting point for the further development and optimization of new and potent G4 ligands.

Experimental

Chemistry

Commercial reagents were used as received without additional purification. Melting points were determined with an SM-LUX-POL Leitz hot-stage microscope and are uncorrected. IR spectra were recorded on a NICOLET 380FT-IR spectrophotometer. NMR spectra were recorded with tetramethylsilane as an internal standard using a BRUKER AVANCE 300 spectrometer. Splitting patterns are designated as follows: s = singlet; bs = broad singlet; d = doublet; t = triplet; q = quartet; dd = double doublet; ddd = double double doublet; dt = double triplet; m = multiplet. Analytical TLC was carried out on 0.25-mm precoated silica gel plates (POLYGRAM SIL G/UV₂₅₄) with visualization of compounds by UV light irradiation. Silica gel 60 (70-230 mesh) was used for column chromatography. Microwave experiments were carried out using a focused microwave reactor (CEM Discover). High-resolution mass spectra (electrospray in positive mode, ESI+) were recorded on a Waters Q-TOF Ultima apparatus. Mass spectra were recorded on an Ultraflex III TOF/TOF system (Bruker Daltonics), equipped with 200 Hz smartbeam laser (355 nm) and operating in reflectron positive ion mode. Mass spectra were acquired over the m/z range 300–5000 by accumulating data from 1000 laser shots for each spectrum. The instrumental conditions employed to analyse molecular species were the following: ion source 1: 25.08 kV; ion source 2: 21.98 kV, lens: 11.03 kV, pulsed ion extraction: 30 ns, reflector: 26.39 kV, reflector 2: 13.79 kV. Matrix suppression was activated by deflection mode: suppression up to 450 Da. Mass calibration was performed for each sample with a peptide calibration mixture (8206195, Peptide Calibration Standard, Bruker Daltonics). The instrument was controlled using Bruker's flexControl 3.4 software, and mass spectra were analysed in Bruker's FlexAnalysis 3.4 software.

General procedure for syntheses of bis-[2,9-(formylphenyl)]-1,10-phenanthrolines **2a-c**

Method A: To a suspension of 2,9-dichloro-1,10-phenanthroline (4 mmol) and Pd(PPh₃)₄ (0.4 mmol) in a mixture of toluene/EtOH (40 mL/2 mL) under nitrogen were added K₂CO₃ (8.8 mmol) and 3- or 4-formylphenylboronic acid (8.8 mmol). The reaction mixture was refluxed for 24 h, and the cooled suspension was extracted with CH₂Cl₂ (3 x 50 mL). The organic layer was washed with a saturated solution of NaCl (70 mL), and the combined organic extracts were dried over sodium sulfate, filtered, and evaporated under reduced pressure. The crude residue was triturated in ethanol. The resulting precipitate was filtered, washed with ethanol, and purified by column chromatography on silica gel using dichloromethane as eluent to give the pure product **2**. **Method B:** To a suspension of 2,9-dichloro-1,10-phenanthroline (4 mmol), 2-, 3- or 4-formylphenylboronic acid (8.8 mmol), and Pd(PPh₃)₄ (0.4 mmol) in DME (40 mL) under nitrogen were added 4 mL of a 2 M aqueous solution of Na₂CO₃. The reaction mixture was refluxed for 24 h. The suspension was then evaporated to dryness and extracted with CH₂Cl₂ (2 x 50 mL). The organic layer was filtered and washed with water (2 x 50 mL). The organic layer was dried over sodium sulfate, filtered, and evaporated under reduced pressure. The crude residue was triturated in ethanol. The resulting precipitate was filtered, washed with ethanol, and purified by column chromatography on silica gel using dichloromethane as eluent to give the pure product **2a-c**.

Bis-[2,9-(3-formylphenyl)]-1,10-phenanthroline **2b**

Beige crystals (71% Method A; 78% Method B); mp=181 °C. ¹H NMR (CDCl₃) δ: 10.28 (s, 2H, 2 CHO), 9.05 (dd, J=1.45 and 1.45 Hz, 2H, 2 H-2'), 8.80 (ddd, J=7.70, 1.45 and 1.45 Hz, 2H, 2 H-6'), 8.42 (d, J=8.40 Hz, 2H, H-4 and H-7), 8.27 (d, J=8.40 Hz, 2H, H-3 and H-8), 8.06 (ddd, J=7.70, 1.45 and 1.45 Hz, 2H, 2 H-4'), 7.89 (s, 2H, H-5 and H-6), 7.81 (t, J=7.70 Hz, 2H, 2 H-5'). ¹³C NMR (CDCl₃) δ: 193.8 (2 C=O), 156.4 (C-2 and C-9), 147.3 (C-1a and C-10a), 141.5 (2 C-3'), 138.6 (C-4 and C-7), 138.3 (2 C-1'), 134.6 (2 C-2'), 131.8 (2 C-5'), 131.0 (2 C-4'), 130.3 (2 C-6'), 129.6 (C-4a and C-6a), 127.8 (C-5 and C-6), 121.1 (C-3 and C-8). HRMS-ESI m/z [M+H]⁺ Calcd for C₂₆H₁₆N₂O₂: 389.1290, Found: 389.1274.

Bis-[2,9-(2-formylphenyl)]-1,10-phenanthroline **2c**

Beige crystals (70% Method B); mp=172 °C. ¹H NMR (CDCl₃) δ: 10.43 (s, 2H, 2 CHO), 8.42 (d, J=8.20 Hz, 2H, H-4 and H-7), 8.10 (dd, J=7.80 and 1.20 Hz, 2H, 2 H-6'), 7.99 (d, J=8.20 Hz, 2H, H-3 and H-8), 7.95 (dd, J=7.80 and 1.20 Hz, 2H, 2 H-3'), 7.94 (s, 2H, H-5 and H-6), 7.75 (ddd, J=7.80 and 1.20 Hz, 2 H-5'), 7.60 (ddd, J=7.80 and 1.20 Hz, 2 H-4'). ¹³C NMR (CDCl₃) δ: 193.8 (2 C=O), 157.6 (C-2 and C-9), 147.2 (C-1a and C-10a), 144.6 (2 C-2'), 138.2 (C-4 and C-7), 137.0 (2 C-1'), 134.5 (2 C-5'), 132.2 (2 C-3'), 130.5 (2 C-6'), 129.9 (2 C-4'), 129.1 (C-4a and C-6a), 128.1 (C-5 and C-6), 125.2 (C-3 and C-8). HRMS-ESI m/z [M+H]⁺ Calcd for C₂₆H₁₆N₂O₂: 389.1290, Found: 389.1286.

Synthesis of 2-(4-Formylphenyl)-1,10-phenanthroline **2d**

Under nitrogen, 4-formylphenylboronic acid, pinacol ester (3.5 mmol), 2-chloro-1,10-phenanthroline (4 mmol), Pd(PPh₃)₄ (0.07 mmol), Cs₂CO₃ (5.8 mmol), and 1,2-dimethoxyethane (23 mL) were mixed, followed by stirring at 80 °C for 6 h. The reaction mixture was then cooled, and water (31 mL) was added to the reaction mixture. After a stirring

for 10 min at 0 °C, the precipitate was removed by filtration to yield an orange solid that was then purified by column chromatography on silica gel using dichloromethane/methanol (90/10: v/v) as eluent to give the pure product **2d**. Orange crystals (60%); mp=171 °C. ¹H NMR (CDCl₃) δ: 10.14 (s, 1H, CHO), 9.27 (dd, *J*=4.35 and 1.80 Hz, 1H, H-9), 8.53 (d, *J*=8.40 Hz, 2H, H-2' and H-6'), 8.38 (d, *J*=8.40 Hz, 1H, H-4), 8.30 (dd, *J*=8.00 and 1.80 Hz, 1H, H-7), 8.17 (d, *J*=8.40 Hz, 1H, H-3), 8.07 (d, *J*=8.40, 2H, H-3' and H-5'), 7.86 (d, *J*=9.00 Hz, 1H, H-6), 7.83 (d, *J*=9.00 Hz, 1H, H-5), 7.69 (dd, *J*=8.00 and 4.35 Hz, 1H, H-8). ¹³C NMR (CDCl₃) δ: 193.6 (C=O), 157.2 (C-2), 151.9 (C-9), 147.6 (C-10a), 147.5 (C-1'), 146.5 (C-4'), 138.5 (C-4), 137.9 (C-1a), 137.7 (C-7), 131.6 (C-3' and C-5'), 130.5 (C-6a), 129.9 (C-2' and C-6'), 129.4 (C-4a), 128.4 (C-5), 127.7 (C-6), 124.5 (C-8), 122.2 (C-3). HRMS-ESI *m/z* [M+H]⁺ Calcd for C₁₉H₁₂N₂O: 285.1028, Found: 285.1018.

General procedure for syntheses of 2,9-bis[(substituted-iminomethyl)phenyl]-1,10-phenanthrolines **3a-i**

To a solution of diamine (2.7 mmol) in ethanol (15 mL) was added bis-[2,9-(2-, 3- or 4-formylphenyl)]-1,10-phenanthroline **2a-c** (1.29 mmol). The reaction mixture was then heated under reflux for 5 h and then evaporated to dryness under reduced pressure. After cooling, the residue was extracted with dichloromethane (40 mL). The organic layer was dried over sodium sulfate and evaporated to dryness. Products were then used without further purification.

2,9-Bis{4-[(3-dimethylaminopropyl)iminomethyl]phenyl}-1,10-phenanthroline **3a**

Orange oil (94%). ¹H NMR (CDCl₃) δ: 8.53 (d, *J*=8.40 Hz, 4H, 2 H-2' and 2 H-6'), 8.41 (s, 2H, 2 HC=N), 8.31 (d, *J*=8.40 Hz, 2H, H-4 and H-7), 8.17 (d, *J*=8.40 Hz, 2H, H-3 and H-8), 7.95 (d, *J*=8.40 Hz, 4H, 2 H-3' and 2 H-5'), 7.79 (s, 2H, H-5 and H-6), 3.72 (t, *J*=7.20 Hz, 4H, 2 NCH₂), 2.42 (t, *J*=7.20 Hz, 4H, 2 NCH₂), 2.28 (s, 12H, 4 CH₃), 1.95 (qt, *J*=7.20 Hz, 4H, 2 CH₂).

2,9-Bis{4-[(3-(4-methylpiperazin-1-yl)propyl)iminomethyl]phenyl}-1,10-phenanthroline **3b**

Orange crystals (98%); mp=124 °C. ¹H NMR (CDCl₃) δ: 8.55 (d, *J*=8.40 Hz, 4H, 2 H-2' and 2 H-6'), 8.42 (s, 2H, 2 HC=N), 8.34 (d, *J*=8.40 Hz, 2H, H-4 and H-7), 8.20 (d, *J*=8.40 Hz, 2H, H-3 and H-8), 7.96 (d, *J*=8.40 Hz, 4H, 2 H-3' and 2 H-5'), 7.83 (s, 2H, H-5 and H-6), 3.74 (t, *J*=7.10 Hz, 4H, 2 NCH₂), 2.62-2.40 (m, 20H, 2 NCH₂ and 8 NCH₂pip.), 2.32 (s, 12H, 4 CH₃), 1.97 (qt, *J*=7.10 Hz, 4H, 2 CH₂).

2,9-Bis{4-[(3-pyrrolidinopropyl)iminomethyl]phenyl}-1,10-phenanthroline **3c**

Yellow oil (98%). ¹H NMR (CDCl₃) δ: 8.56 (d, *J*=8.40 Hz, 4H, 2 H-2' and 2 H-6'), 8.43 (s, 2H, 2 HC=N), 8.35 (d, *J*=8.40 Hz, 2H, H-4 and H-7), 8.21 (d, *J*=8.40 Hz, 2H, H-3 and H-8), 7.97 (d, *J*=8.40 Hz, 4H, 2 H-3' and 2 H-5'), 7.83 (s, 2H, H-5 and H-6), 3.76 (t, *J*=7.20 Hz, 4H, 2 NCH₂), 2.61 (t, *J*=7.20 Hz, 4H, 2 NCH₂), 2.62-2.54 (m, 8H, 4 NCH₂pyrrol.), 2.01 (qt, *J*=7.20 Hz, 4H, 2 CH₂), 1.85-1.79 (m, 8H, 4 CH₂pyrrol.).

2,9-Bis{4-[(3-morpholinopropyl)iminomethyl]phenyl}-1,10-phenanthroline **3d**

Orange oil (97%). ¹H NMR (CDCl₃) δ: 8.55 (d, *J*=8.40 Hz, 4H, 2 H-2' and 2 H-6'), 8.42 (s, 2H, 2 HC=N), 8.35 (d, *J*=8.40 Hz, 2H, H-4 and H-7), 8.21 (d, *J*=8.40 Hz, 2H, H-3 and H-8), 7.95 (d, *J*=8.40 Hz, 4H, 2 H-3' and 2 H-5'), 7.83 (s, 2H, H-5 and H-6), 3.78-3.69 (m, 12H, 4 OCH₂ and 2 NCH₂), 2.54-2.42 (m, 12H, 2 NCH₂ and 4 NCH₂morph.), 1.97 (qt, *J*=7.20 Hz, 4H, 2 CH₂).

2,9-Bis{3-[(3-dimethylaminopropyl)iminomethyl]phenyl}-1,10-phenanthroline **3e**

Orange oil (90%). ¹H NMR (CDCl₃) δ: 8.73-8.69 (m, 4H, 2 H-2' and 2 H-6'), 8.50 (s, 2H, HC=N), 8.37 (d, *J*=8.40 Hz, 2H, H-4 and H-7), 8.27 (d, *J*=8.40 Hz, 2H, H-3 and H-8), 7.90 (ddd, *J*=7.90, 1.20 and 1.20 Hz, 2H, 2 H-4'), 7.85 (s, 2H, H-5 and H-6), 7.69 (t, *J*=7.90 Hz, 2H, 2 H-5'), 3.75 (t, *J*=7.20 Hz, 4H, 2 NCH₂), 2.42 (t, *J*=7.20 Hz, 4H, 2 NCH₂), 2.26 (s, 12H, 4 CH₃), 1.96 (qt, *J*=7.20 Hz, 4H, 2 CH₂).

2,9-Bis{3-[(3-(4-methylpiperazin-1-yl)propyl)iminomethyl]phenyl}-1,10-phenanthroline **3f**

Orange oil (96%). ¹H NMR (CDCl₃) δ: 8.72-8.69 (m, 4H, 2 H-2' and 2 H-6'), 8.48 (s, 2H, HC=N), 8.36 (d, *J*=8.40 Hz, 2H, H-4 and H-7), 8.26 (d, *J*=8.40 Hz, 2H, H-3 and H-8), 7.89 (ddd, *J*=7.60, 1.30 and 1.30 Hz, 2H, 2 H-4'), 7.84 (s, 2H, H-5 and H-6), 7.65 (t, *J*=7.60 Hz, 2H, 2 H-5'), 3.74 (t, *J*=7.10 Hz, 4H, 2 NCH₂), 2.53-2.28 (m, 20H, 2 NCH₂ and 16 NCH₂pip.), 2.29 (s, 6H, 2 CH₃), 1.97 (qt, *J*=7.10 Hz, 4H, 2 CH₂).

2,9-Bis{3-[(3-pyrrolidinopropyl)iminomethyl]phenyl}-1,10-phenanthroline 3g

Yellow oil (98%). ¹H NMR (CDCl₃) δ: 8.73-8.68 (m, 4H, 2 H-2' and 2 H-6'), 8.49 (s, 2H, HC=N), 8.36 (d, *J*=8.40 Hz, 2H, H-4 and H-7), 8.26 (d, *J*=8.40 Hz, 2H, H-3 and H-8), 7.90 (ddd, *J*=7.80, 1.20 and 1.20 Hz, 2H, 2 H-4'), 7.84 (s, 2H, H-5 and H-6), 7.68 (t, *J*=7.80 Hz, 2H, 2 H-5'), 3.77 (t, *J*=7.10 Hz, 4H, 2 NCH₂), 2.61 (t, *J*=7.10 Hz, 4H, 2 NCH₂), 2.61-2.54 (m, 8H, 4 NCH₂pyrrol.), 2.02 (qt, *J*=7.10 Hz, 4H, 2 CH₂), 1.84-1.79 (m, 8H, 4 NCH₂pyrrol.).

2,9-Bis{2-[(3-dimethylaminopropyl)iminomethyl]phenyl}-1,10-phenanthroline 3h

Orange oil (98%). ¹H NMR (CDCl₃) δ: 8.78 (s, 2H, HC=N), 8.36 (d, *J*=8.10 Hz, 2H, H-4 and H-7), 8.13 (dd, *J*=7.50 and 1.80 Hz, 2H, 2 H-6'), 7.91 (s, 2H, H-5 and H-6), 7.84 (dd, *J*=7.50 and 1.80 Hz, 2H, 2 H-3'), 7.81 (d, *J*=8.10 Hz, 2H, H-3 and H-8), 7.56 (ddd, *J*=7.50 and 1.80 Hz, 2H, 2 H-5'), 7.50 (ddd, *J*=7.50 and 1.80 Hz, 2H, 2 H-4'), 3.55 (t, *J*=7.10 Hz, 4H, 2 NCH₂), 2.25 (t, *J*=7.10 Hz, 4H, 2 NCH₂), 2.18 (s, 12H, 4 CH₃), 1.82 (qt, *J*=7.10 Hz, 4H, 2 CH₂).

2,9-Bis{2-[(3-(4-methylpiperazin-1-yl)propyl)iminomethyl]phenyl}-1,10-phenanthroline 3i

Orange oil (98%). ¹H NMR (CDCl₃) δ: 8.81 (s, 2H, HC=N), 8.35 (d, *J*=8.40 Hz, 2H, H-4 and H-7), 8.13 (dd, *J*=7.50 and 1.50 Hz, 2H, 2 H-6'), 7.91 (s, 2H, H-5 and H-6), 7.84 (dd, *J*=7.50 and 1.50 Hz, 2H, 2 H-3'), 7.82 (d, *J*=8.40 Hz, 2H, H-3 and H-8), 7.57 (ddd, *J*=7.50 and 1.50 Hz, 2H, 2 H-5'), 7.51 (ddd, *J*=7.50 and 1.80 Hz, 2H, 2 H-4'), 3.54 (t, *J*=6.90 Hz, 4H, 2 NCH₂), 2.48-2.28 (m, 20H, 2 NCH₂ and 16 NCH₂pip.), 2.24 (s, 6H, 2 CH₃), 1.83 (qt, *J*=6.90 Hz, 4H, 2 CH₂).

Synthesis of 2-[4-[(3-Dimethylaminopropyl)iminomethyl]phenyl]-1,10-phenanthroline 3j

To a solution of diamine (0.44 mmol) in ethanol (6 mL) was added 2-(4-formylphenyl)-1,10-phenanthroline **2d** (0.42 mmol). The reaction mixture was heated under reflux for 5 h and then evaporated to dryness under reduced pressure. After cooling, the residue was extracted with dichloromethane (25 mL). The organic layer was dried over sodium sulfate and evaporated to dryness. Products were then used without further purification. Yellow oil (97%). ¹H NMR (CDCl₃) δ: 9.19 (dd, *J*=4.40 and 1.80 Hz, 1H, H-9), 8.36 (d, *J*=8.40 Hz, 2H, H-2' and H-6'), 8.33 (s, 1H, HC=N), 8.20 (d, *J*=8.40 Hz, 1H, H-4), 8.16 (dd, *J*=8.10 and 1.80 Hz, 1H, H-7), 8.03 (d, *J*=8.40 Hz, 1H, H-3), 7.86 (d, *J*=8.40, 2H, H-3' and H-5'), 7.70 (d, *J*=8.70 Hz, 1H, H-6), 7.67 (d, *J*=8.70 Hz, 1H, H-5), 7.57 (dd, *J*=8.10 and 4.40 Hz, 1H, H-8), 3.65 (t, *J*=7.10 Hz, 4H, 2 NCH₂), 2.35 (t, *J*=7.10 Hz, 4H, 2 NCH₂), 2.21 (s, 12H, 4 CH₃), 1.88 (qt, *J*=7.10 Hz, 4H, 2 CH₂).

General procedure for syntheses of 2,9-bis[(substituted-aminomethyl)phenyl]-1,10-phenanthrolines 1a-i

To a solution of compound **3a-i** (1.26 mmol) in methanol (40 mL) was added portion-wise at 0 °C sodium borohydride (10.1 mmol; 8 equiv.). The reaction mixture was then heated under reflux for 4 h and then evaporated to dryness under reduced pressure. After cooling, the residue was triturated in water and extracted with dichloromethane (85 mL). The organic layer was separated, dried over sodium sulfate, and evaporated to dryness. The residue was then purified by column chromatography on silica gel using dichloromethane/methanol (90/10, v/v) as eluent to give the pure product **1**.

2,9-Bis{4-[(3-dimethylaminopropyl)aminomethyl]phenyl}-1,10-phenanthroline 1a

Yellow oil (83%). ¹H NMR (CDCl₃) δ: 8.45 (d, *J*=8.40 Hz, 4H, 2 H-2' and 2 H-6'), 8.32 (d, *J*=8.55 Hz, 2H, H-4 and H-7), 8.16 (d, *J*=8.55 Hz, 2H, H-3 and H-8), 7.81 (s, 2H, H-5 and H-6), 7.56 (d, *J*=8.40 Hz, 4H, 2 H-3' and 2 H-5'), 3.95 (s, 4H, 2 NCH₂), 2.77 (t, *J*=7.05 Hz, 4H, 2 NCH₂), 2.38 (t, *J*=7.05 Hz, 4H, 2 NCH₂), 2.31 (bs, 2H, 2 NH), 2.25 (s, 12H, 4 CH₃), 1.76 (qt, *J*=7.05 Hz, 4H, 2 CH₂). ¹³C NMR (CDCl₃) δ: 158.0 (C-2 and C-9), 147.4 (C-1a and C-10a), 143.1 (2 C-4'), 139.6 (2 C-1'), 138.2 (C-4 and C-7), 130.0 (2 C-3' and 2 C-5'), 129.2 (C-4a and C-6a), 129.1 (2 C-2' and 2 C-6'), 127.3 (C-5 and C-6), 121.3 (C-3 and C-8), 59.4 (2 NCH₂), 55.1 (2 NCH₂), 49.2 (2 NCH₂), 46.9 (4 CH₃), 29.3 (2 CH₂). MALDI-TOF MS *m/z* [M+H]⁺ Calcd for C₃₆H₄₅N₆: 561.371, Found: 561.425.

2,9-Bis{4-[(3-(4-methylpiperazin-1-yl)propyl)aminomethyl]phenyl}-1,10-phenanthroline 1b

Yellow oil (81%). ¹H NMR (CDCl₃) δ: 8.40 (d, *J*=8.40 Hz, 4H, 2 H-2' and 2 H-6'), 8.26 (d, *J*=8.55 Hz, 2H, H-4 and H-7), 8.10 (d, *J*=8.55 Hz, 2H, H-3 and H-8), 7.74 (s, 2H, H-5 and H-6), 7.52 (d, *J*=8.40 Hz, 4H, 2 H-3' and 2 H-5'), 3.88 (s, 4H, 2 NCH₂), 2.71 (t, *J*=7.05 Hz, 4H, 2 NCH₂), 2.60-2.29 (m, 22H, 2 NCH₂, 2 NH and 8 NCH₂pip.), 2.26 (s, 6H, 2 CH₃), 1.73 (qt, *J*=7.05 Hz, 4H, 2 CH₂). ¹³C NMR (CDCl₃) δ: 158.0 (C-2 and C-9), 147.4 (C-1a and C-10a), 143.1 (2 C-

4'), 139.5 (2 C-1'), 138.3 (C-4 and C-7), 129.9 (2 C-3' and 2 C-5'), 129.2 (C-4a and C-6a), 129.1 (2 C-2' and 2 C-6'), 127.3 (C-5 and C-6), 121.3 (C-3 and C-8), 58.4 (2 NCH₂), 56.5 (4 NCH₂pip.), 55.1 (2 NCH₂), 54.6 (4 NCH₂pip.), 49.4 (2 NCH₂), 47.4 (2 CH₃), 28.3 (2 CH₂). MALDI-TOF MS m/z [M+H]⁺ Calcd for C₄₂H₅₅N₈: 671.455, Found: 671.524.

2,9-Bis{4-[(3-pyrrolidinopropyl)aminomethyl]phenyl}-1,10-phenanthroline 1c

Yellow oil (93%). ¹H NMR (CDCl₃) δ: 8.43 (d, *J*=8.10 Hz, 4H, 2 H-2' and 2 H-6'), 8.26 (d, *J*=8.40 Hz, 2H, H-4 and H-7), 8.12 (d, *J*=8.40 Hz, 2H, H-3 and H-8), 7.74 (s, 2H, H-5 and H-6), 7.53 (d, *J*=8.10 Hz, 4H, 2 H-3' and 2 H-5'), 3.91 (s, 4H, 2 NCH₂), 2.74 (t, *J*=6.90 Hz, 4H, 2 NCH₂), 2.55-2.47 (m, 12H, 2 NCH₂ and 4 NCH₂pyrrol.), 2.05 (bs, 2H, 2 NH), 1.84-1.72 (m, 12H, 2 CH₂ and 4 CH₂pyrrol.). ¹³C NMR (CDCl₃) δ: 158.0 (C-2 and C-9), 147.4 (C-1a and C-10a), 143.1 (2 C-4'), 139.5 (2 C-1'), 138.3 (C-4 and C-7), 129.9 (2 C-3' and 2 C-5'), 129.2 (C-4a and C-6a), 129.1 (2 C-2' and 2 C-6'), 127.3 (C-5 and C-6), 121.3 (C-3 and C-8), 56.2 (2 NCH₂), 55.6 (4 NCH₂), 55.1 (2 NCH₂), 49.3 (2 NCH₂), 30.5 (2 CH₂), 24.8 (4 CH₂). MALDI-TOF MS m/z [M+H]⁺ Calcd for C₄₀H₄₉N₆: 613.402, Found: 613.546.

2,9-Bis{4-[(3-morpholinopropyl)aminomethyl]phenyl}-1,10-phenanthroline 1d

Yellow oil (77%). ¹H NMR (CDCl₃) δ: 8.45 (d, *J*=8.40 Hz, 4H, 2 H-2' and 2 H-6'), 8.34 (d, *J*=8.40 Hz, 2H, H-4 and H-7), 8.17 (d, *J*=8.40 Hz, 2H, H-3 and H-8), 7.82 (s, 2H, H-5 and H-6), 7.57 (d, *J*=8.40 Hz, 4H, 2 H-3' and 2 H-5'), 3.96 (s, 4H, 2 NCH₂), 3.73 (t, *J*=4.80 Hz, 8H, 4 OCH₂), 2.81 (t, *J*=6.90 Hz, 4H, 2 NCH₂), 2.54-2.42 (m, 12H, 2 NCH₂ and 4 NCH₂morph.), 1.80 (qt, *J*=6.90 Hz, 6H, 2 NH and 2 CH₂). ¹³C NMR (CDCl₃) δ: 158.0 (C-2 and C-9), 147.5 (C-1a and C-10a), 142.9 (2 C-4'), 139.6 (2 C-1'), 138.3 (C-4 and C-7), 130.0 (2 C-3' and 2 C-5'), 129.3 (C-4a and C-6a), 129.1 (2 C-2' and 2 C-6'), 127.4 (C-5 and C-6), 121.3 (C-3 and C-8), 68.4 (4 OCH₂), 58.9 (2 NCH₂), 55.2 (2 NCH₂), 55.1 (4 NCH₂), 49.3 (2 NCH₂), 27.9 (2 CH₂). MALDI-TOF MS m/z [M+H]⁺ Calcd for C₄₀H₄₉N₆O₂: 645.392, Found: 645.469.

2,9-Bis{3-[(3-dimethylaminopropyl)aminomethyl]phenyl}-1,10-phenanthroline 1e

Yellow oil (77%). ¹H NMR (CDCl₃) δ: 8.42 (dd, *J*=1.40 and 1.40 Hz, 2H, 2 H-2'), 8.40 (ddd, *J*=7.50, 1.40 and 1.40 Hz, 2H, 2 H-6'), 8.32 (d, *J*=8.40 Hz, 2H, H-4 and H-7), 8.18 (d, *J*=8.40 Hz, 2H, H-3 and H-8), 7.81 (s, 2H, H-5 and H-6), 7.57 (t, *J*=7.50 Hz, 2H, 2 H-5'), 7.48 (ddd, *J*=7.50, 1.40 and 1.40 Hz, 2H, 2 H-4'), 3.99 (s, 4H, 2 NCH₂), 2.76 (t, *J*=7.20 Hz, 4H, 2 NCH₂), 2.35 (t, *J*=7.20 Hz, 4H, 2 NCH₂), 2.28 (bs, 2H, 2 NH), 2.22 (s, 12H, 4 CH₃), 1.74 (qt, *J*=7.20 Hz, 4H, 2 CH₂). ¹³C NMR (CDCl₃) δ: 158.1 (C-2 and C-9), 147.4 (C-1a and C-10a), 142.1 (2 C-3'), 140.9 (2 C-1'), 138.3 (C-4 and C-7), 130.7 (2 C-2'), 130.3 (2 C-5'), 129.3 (C-4a and C-6a), 128.9 (2 C-4'), 127.8 (2 C-6'), 127.4 (C-5 and C-6), 121.5 (C-3 and C-8), 59.4 (2 NCH₂), 55.6 (2 NCH₂), 49.2 (2 NCH₂), 46.9 (4 CH₃), 29.4 (2 CH₂). MALDI-TOF MS m/z [M+H]⁺ Calcd for C₃₆H₄₅N₆: 561.371, Found: 561.460.

2,9-Bis{3-[(3-(4-methylpiperazin-1-yl)propyl)aminomethyl]phenyl}-1,10-phenanthroline 1f

Yellow oil (67%). ¹H NMR (CDCl₃) δ: 8.42 (dd, *J*=1.30 and 1.30 Hz, 2H, 2 H-2'), 8.37 (ddd, *J*=7.50, 1.30 and 1.30 Hz, 2H, 2 H-6'), 8.32 (d, *J*=8.40 Hz, 2H, H-4 and H-7), 8.18 (d, *J*=8.40 Hz, 2H, H-3 and H-8), 7.81 (s, 2H, H-5 and H-6), 7.56 (t, *J*=7.50 Hz, 2H, 2 H-5'), 7.47 (ddd, *J*=7.50, 1.30 and 1.30 Hz, 2H, 2 H-4'), 3.98 (s, 4H, 2 NCH₂), 2.76 (t, *J*=7.10 Hz, 4H, 2 NCH₂), 2.55-2.30 (m, 22H, 2 NCH₂, 2 NH and 16 NCH₂pip.), 2.23 (s, 6H, 2 CH₃), 1.75 (qt, *J*=7.10 Hz, 4H, 2 CH₂). ¹³C NMR (CDCl₃) δ: 158.1 (C-2 and C-9), 147.4 (C-1a and C-10a), 142.1 (2 C-3'), 140.9 (2 C-1'), 138.3 (C-4 and C-7), 130.7 (2 C-2'), 130.3 (2 C-5'), 129.3 (C-4a and C-6a), 128.9 (2 C-4'), 127.7 (2 C-6'), 127.4 (C-5 and C-6), 121.5 (C-3 and C-8), 58.4 (2 NCH₂), 56.4 (4 NCH₂pip.), 55.6 (2 NCH₂), 54.6 (4 NCH₂pip.), 49.5 (2 NCH₂), 47.3 (2 CH₃), 28.3 (2 CH₂). MALDI-TOF MS m/z [M+H]⁺ Calcd for C₄₂H₅₅N₈: 671.455, Found: 671.529.

2,9-Bis{3-[(3-pyrrolidinopropyl)aminomethyl]phenyl}-1,10-phenanthroline 1g

Yellow oil (74%). ¹H NMR (CDCl₃) δ: 8.42 (dd, *J*=1.30 and 1.30 Hz, 2H, 2 H-2'), 8.38 (ddd, *J*=7.50, 1.30 and 1.30 Hz, 2H, 2 H-6'), 8.32 (d, *J*=8.40 Hz, 2H, H-4 and H-7), 8.17 (d, *J*=8.40 Hz, 2H, H-3 and H-8), 7.80 (s, 2H, H-5 and H-6), 7.56 (t, *J*=7.50 Hz, 2H, 2 H-5'), 7.48 (ddd, *J*=7.50, 1.30 and 1.30 Hz, 2H, 2 H-4'), 3.99 (s, 4H, 2 NCH₂), 2.77 (t, *J*=7.10 Hz, 4H, 2 NCH₂), 2.56-2.45 (m, 12H, 2 NCH₂ and 4 NCH₂pyrrol.), 2.26 (bs, 2H, 2 NH), 1.83-1.72 (m, 12H, 2 CH₂ and 4 CH₂pyrrol.). ¹³C NMR (CDCl₃) δ: 158.1 (C-2 and C-9), 147.4 (C-1a and C-10a), 142.2 (2 C-3'), 140.9 (2 C-1'), 138.3 (C-4 and C-7), 130.6 (2 C-2'), 130.3 (2 C-5'), 129.3 (C-4a and C-6a), 128.9 (2 C-4'), 127.7 (2 C-6'), 127.4 (C-5

and C-6), 121.5 (C-3 and C-8), 56.1 (2 NCH₂), 55.6 (4 NCH₂), 55.5 (2 NCH₂), 49.4 (2 NCH₂), 30.6 (2 CH₂), 24.8 (4 CH₂). MALDI-TOF MS m/z [M+H]⁺ Calcd for C₄₀H₄₉N₆: 613.402, Found: 613.510.

2,9-Bis{2-[(3-dimethylaminopropyl)aminomethyl]phenyl}-1,10-phenanthroline **1h**

Yellow-orange oil (97%). ¹H NMR (CDCl₃) δ: 8.37 (d, *J*=8.10 Hz, 2H, H-4 and H-7), 7.88 (s, 2H, H-5 and H-6), 7.87 (d, *J*=8.10 Hz, 2H, H-3 and H-8), 7.62-7.59 (m, 2H, 2 H-6'), 7.56-7.51 (m, 2H, 2 H-3'), 7.45-7.40 (m, 4H, 2 H-4' and 2 H-5'), 3.65 (s, 4H, 2 NCH₂), 2.36 (t, *J*=7.20 Hz, 4H, 2 NCH₂), 1.98 (s, 12H, 4 CH₃), 1.92 (t, *J*=7.20 Hz, 4H, 2 NCH₂), 1.23 (qt, *J*=7.20 Hz, 4H, 2 CH₂). ¹³C NMR (CDCl₃) δ: 160.9 (C-2 and C-9), 146.6 (C-1a and C-10a), 142.6 (2 C-2'), 139.7 (2 C-1'), 138.0 (C-4 and C-7), 132.9 (2 C-3'), 131.5 (2 C-5'), 130.0 (2 C-6'), 128.8 (C-4a and C-6a), 128.6 (2 C-4'), 127.6 (C-5 and C-6), 125.1 (C-3 and C-8), 59.1 (2 NCH₂), 53.1 (2 NCH₂), 48.1 (2 NCH₂), 46.7 (4 CH₃), 28.2 (2 CH₂). MALDI-TOF MS m/z [M+H]⁺ Calcd for C₃₆H₄₅N₆: 561.371, Found: 561.384.

2,9-Bis{2-[(3-(4-methylpiperazin-1-yl)propyl)aminomethyl]phenyl}-1,10-phenanthroline **1i**

Yellow oil (98%). ¹H NMR (CDCl₃) δ: 8.35 (d, *J*=8.10 Hz, 2H, H-4 and H-7), 7.88 (d, *J*=8.10 Hz, 2H, H-3 and H-8), 7.87 (s, 2H, H-5 and H-6), 7.62-7.59 (m, 2H, 2 H-6'), 7.55-7.50 (m, 2H, 2 H-3'), 7.45-7.40 (m, 4H, 2 H-4' and 2 H-5'), 3.66 (s, 4H, 2 NCH₂), 2.45-2.15 (m, 22H, 2 NCH₂, 2 NH and 16 NCH₂pip.), 2.18 (s, 6H, 2 CH₃), 2.00 (t, *J*=6.90 Hz, 4H, 2 NCH₂), 1.29 (qt, *J*=6.90 Hz, 4H, 2 CH₂). ¹³C NMR (CDCl₃) δ: 161.0 (C-2 and C-9), 146.7 (C-1a and C-10a), 142.5 (2 C-2'), 141.7 (2 C-1'), 137.9 (C-4 and C-7), 132.8 (2 C-3'), 131.5 (2 C-5'), 129.9 (2 C-6'), 128.7 (C-4a and C-6a), 128.5 (2 C-4'), 127.6 (C-5 and C-6), 125.1 (C-3 and C-8), 58.0 (2 NCH₂), 56.4 (4 NCH₂pip.), 54.4 (4 NCH₂pip.), 53.1 (2 NCH₂), 48.2 (2 NCH₂), 47.4 (2 CH₃), 27.6 (2 CH₂). MALDI-TOF MS m/z [M+H]⁺ Calcd for C₄₂H₅₅N₈: 671.455, Found: 671.502.

2-{4-[(3-Dimethylaminopropyl)aminomethyl]phenyl}-1,10-phenanthroline **1j**

To a solution of compound **3j** (0.4 mmol) in methanol (6 mL) was added portion-wise at 0 °C sodium borohydride (1.6 mmol; 4 equiv.). The reaction mixture was heated under reflux for 3 h and then evaporated to dryness under reduced pressure. After cooling, the residue was extracted with dichloromethane (25 mL). The organic layer was dried over sodium sulfate and evaporated to dryness to give **1j**. This product was then used without further purification. Yellow oil (95%). ¹H NMR (CDCl₃) δ: 9.20 (dd, *J*=4.20 and 1.80 Hz, 1H, H-9), 8.29 (d, *J*=8.40 Hz, 2H, H-2' and H-6'), 8.23 (d, *J*=8.40 Hz, 1H, H-4), 8.20 (dd, *J*=8.10 and 1.80 Hz, 1H, H-7), 8.05 (d, *J*=8.40 Hz, 1H, H-3), 7.75 (d, *J*=8.70 Hz, 1H, H-6), 7.70 (d, *J*=8.70 Hz, 1H, H-5), 7.60 (dd, *J*=8.10 and 4.20 Hz, 1H, H-8), 7.47 (d, *J*=8.40, 2H, H-3' and H-5'), 3.86 (s, 2H, NCH₂), 2.68 (t, *J*=7.20 Hz, 2H, NCH₂), 2.32 (t, *J*=7.20 Hz, 2H, NCH₂), 2.21 (s, 6H, 2 CH₃), 1.69 (qt, *J*=7.20 Hz, 2H, CH₂). ¹³C NMR (CDCl₃) δ: 158.7 (C-2), 151.6 (C-9), 147.7 (C-10a), 147.4 (C-4'), 143.0 (C-1a), 139.7 (C-1'), 138.2 (C-4), 137.5 (C-7), 130.4 (C-6a), 129.9* (C-3' and C-5'), 129.4 (C-2' and C-6'), 128.8 (C-4a), 127.7 (C-5), 127.5 (C-6), 124.2 (C-8), 121.9 (C-3), 59.4 (NCH₂), 55.1 (NCH₂), 49.1 (NCH₂), 46.9 (2 CH₃), 29.3 (CH₂). MALDI-TOF MS m/z [M+H]⁺ Calcd for C₂₄H₂₆N₄: 370.216, Found: 371.088.

General procedure for preparation of 2,9-bis[4-(substituted-aminomethyl)phenyl]-1,10-phenanthrolines and 2-{4-[(3-Dimethylaminopropyl)aminomethyl]phenyl}-1,10-phenanthroline oxalate salts

To a solution of compounds **1a-j** (1 mmol) in isopropanol (35 mL) was added oxalic acid (8 or 4 mmol). The reaction mixture was heated under reflux for 30 min. The precipitate was filtered, washed with isopropanol then with diethyl ether and dried under reduced pressure to give the ammonium salts of **1a-j**.

X-ray data

The structure of compound **2b** was established by X-ray crystallography (Figure 2). A colourless single crystal of **2b** was obtained by slow evaporation from a methanol/chloroform solution (v/v : 20/80) : triclinic, space group P2₁/c, *a*=3.85830(10) Å, *b*=27.5209(11) Å, *c*=17.5367(7) Å, α=90°, β=91.0803(17)°, γ=90°, *V*=1861.78(12)Å³, *Z*=4, δ(calcd)=1.450 Mg.m⁻³, FW=406.42 for C₂₆H₁₆N₂O₂·H₂O, *F*(000)=848. Full crystallographic results have been deposited at the Cambridge Crystallographic Data Centre (CCDC-1439636), UK, as supplementary material^[55]. The data were corrected for Lorentz and polarization effects and for empirical absorption correction^[56]. The structure was solved by direct methods and refined using Shelx 2013 suite of programs^[56].

Solubility of compounds

Stock solutions of all compounds were prepared at 2 mM and stored at -20 °C. When compounds were not soluble in DMSO at this concentration, the derivatives were diluted in water.

Oligonucleotides

Synthetic oligonucleotides used in this study were purchased from Eurogentec. Stock solutions were prepared in water at concentrations between 100 and 500 μM and stored at $-20\text{ }^{\circ}\text{C}$. Concentrations were determined by quantification of absorbance at 260 nm and using the molar coefficient extinction provided by the manufacturer. The sequences used are listed in Supplementary Table 1. All nucleotides were folded before use in all experiments, typically in the salts conditions indicated, by heating for 5 min at $90\text{ }^{\circ}\text{C}$ and then either slow cooling to room temperature or quick cooling on ice.

FRET melting assays

The FRET melting method is based on the fluorescence resonance energy transfer (FRET) phenomenon between two dyes: a donor and an acceptor (here: 5' FAM and 3' TAMRA). When the nucleotides are folded at low temperature the fluorescence emission of the donor will be minimal due to the acceptor proximity. Fluorescence emission recovery will occur when temperature is increased during the thermally induced melting of the structure. Fluorescence recording was performed in a Strategene MX3005P real-time PCR device at temperatures from 25 to $90\text{ }^{\circ}\text{C}$ using a 492-nm excitation wavelength and a 516-nm detection wavelength. Experiments were performed in 96-well plates, and each condition was tested in duplicate. In each well, 200 nM of labelled oligonucleotide was melted in the presence (or not) of the ligand with (or without) the competitor at concentrations specified.

To determine whether the ligands stabilized the G-quadruplex conformations, we determine the temperature of half denaturation of the G4 in the absence and in the presence of increasing ligand concentrations. For this experiment we used F21T. The oligonucleotide was prefolded in 10 mM lithium cacodylate buffer (pH 7.2), with either 10 mM KCl and 90 mM LiCl (K^+ condition) or 100 mM NaCl (Na^+ condition) as previously described [57]. The salt conditions of the experiment were similar to the one used for the G4 refolding. In addition to the labelled oligonucleotide, the wells contained 0, 1, 2, or 5 μM ligand. To determine ligand G4 vs. duplex selectivity, an unlabelled DNA competitor ds26 was used. The G4 versus duplex selectivity experiments were performed in K^+ conditions using F21T. Wells contained F21T, 1 μM ligand, and 0, 3, or 10 μM unlabelled competitor ds26. Finally, in order to identify a putative preferred G4 conformation targeted by a ligand, a set of oligonucleotides covering a range of possible G4 conformations was used [40]. For the RNA, the KCl concentration was 1 mM and the LiCl concentration was 99 mM [46].

Circular dichroism (CD) spectroscopy

CD was employed to assess conformational changes induced by ligand binding. Melting experiments were also performed with unlabelled sequences to exclude direct dye-ligand interactions. CD experiments were performed on a Jasco J-815 device. CD spectra were the average of three scans, recorded in the wavelength range 230-335 nm at $20\text{ }^{\circ}\text{C}$ at a scan speed of 50 nm/min. The response time was 1 sec, the data pitch was 0.5 nm and the band width was fixed at 2 nm. Buffer conditions were 10 mM lithium cacodylate (pH 7.2), either with 10 mM KCl and 90 mM LiCl (K^+ conditions) or 100 mM NaCl (Na^+ conditions) concentrations. The CD spectrum of the buffer alone was subtracted from each spectrum. The DNA concentration was 3 μM and titrations were performed adding 1 to 5 eq of the ligand under investigation.

For melting experiments, oligonucleotides were prefolded by heating for 5 min at $90\text{ }^{\circ}\text{C}$ and then slowly cooling to room temperature without ligand or with the indicated amount of the ligand. The temperature range for the melting analysis was 4 to $95\text{ }^{\circ}\text{C}$, and the heating rate was $1\text{ }^{\circ}\text{C}/\text{min}$. Changes in the CD signal between 230 and 335 nm were followed at a scan speed of 100 nm/min and with a data pitch of 0.2 nm. Each melting experiment was performed at least 3 times.

Mass spectrometry

The stoichiometry was obtained by electrospray-mass spectrometry in negative ion mode on a Waters LCT Premier mass spectrometer. The ESI source voltage was 2.2 kV, and the sample cone voltage 200 V. The source temperature was set to $60\text{ }^{\circ}\text{C}$. The source voltage was increased to 45 mbar and measured using a Center Two probe (Oerlikon Leybold Vacuum). The syringe injection flow rate is 200 $\mu\text{L}/\text{h}$. These parameters ensured a good signal intensity without disruption of the non-covalent complexes. Note that K^+/DNA or $\text{Ligand}^n/\text{DNA}$ complexes or adducts do not disrupt easily upon collision-induced activation. Trimethylammonium acetate (TMAA, Ultra for UPLC, Fluka) and

potassium chloride (KCl, >99.99%, Sigma) were purchased from Sigma-Aldrich. The injected solutions were prepared diluting the proper volume of the oligonucleotide stock solutions to reach 10 μ M DNA, 100 mM TMAA, and 1 mM KCl supplemented by the mentioned amount of ligand. An annealing at 85 °C followed by a cooling to room temperature was done 24 h before the mass spectrometry experiments.

Fluorescent-based helicase assay using Pif1 from *Saccharomyces cerevisiae*

This assay was used to assess the ability of putative G4 ligands to interfere with the helicase activity of Pif1. This assay was performed using Tecan Infinite M1000PRO micro-plate reader device in black 96-wells plates (Greiner Bio-one). Buffer conditions were 20 mM Tris-HCl (pH 7.2), 5 mM MgCl₂, 1 mM KCl, and 99 mM NaCl. In this assay, the state of a FAM-Dabcyl labelled oligonucleotide system is followed as it is directly correlated to the helicase activity of Pif1. Each oligonucleotide system is composed of a single-stranded region (here including 11 adenosines) that is required for the 5' to 3' Pif1 activity, a central G-quadruplex, and a labelled duplex. Experiments were carried out at 25 °C using 492-nm excitation wavelength and 520-nm emission wavelength to follow the FAM fluorescence emission. Each experiment was performed at least three times. In each well, 20 nM of Pif1 was added to 40 nM DNA, and 5 μ M ATP with or without 1 μ M ligand as previously described [54]. The oligonucleotides are listed in Supplementary Table 1 and included dabcy-l-labelled S-mut, S-dx, S-cmyc, S25ceb, and S-tba. Ss-FAM is a short single-stranded FAM-labelled oligonucleotide that is complementary to the 3'-most 15 nucleotides of the dabcy-l-labelled strand. We also used the complementary non-labelled oligonucleotides of each of the dabcy-l-labelled oligonucleotide to trap them.

Biology

Cell culture

The K562 and HL60 cells were grown in RPMI 1640 medium (Life Technology) supplemented with 10% fetal calf serum, antibiotics (100 U/mL penicillin, 100 μ g/mL streptomycin), and L-glutamine (Eurobio) at 37 °C, 5% CO₂ in air. The cytotoxicities of G4 ligands were also evaluated in freshly isolated normal human peripheral blood mononuclear cells activated with phytohemagglutinin (PHA). Blood from healthy volunteers was centrifuged through a Ficoll gradient to isolate mononuclear cells. Cells were then incubated in medium alone or induced to enter cell cycle by the addition of PHA (5 μ g/mL, Murex Biotech Limited).

Cytotoxicity test

The MTS cell proliferation assay (Promega) is a colorimetric assay that measures the reduction of the tetrazolium MTS into formazan by the mitochondria of viable cells. Cells were washed twice in PBS and plated in quadruplicate into microtiter plate wells in 100 μ L culture media with or without G4 ligand at concentrations of 1, 5, 10, 20, and 50 μ M for 3 days. After 3 hours of incubation at 37 °C with 20 μ L MTS per well, the plates were read using an ELISA microplate reader (Thermo, Electrocorporation) at 490 nm. The amount of colour produced was directly proportional to the number of viable cells. The results are expressed as the concentrations inhibiting cell growth by 50% after a 3 day incubation period. The IC₅₀ was determined by linear regression analysis (Microsoft Excel) and is expressed in μ M \pm SD.

Molecular docking:

Molecular docking was performed using Autodock (Version 4.2) docking software. The molecular structure of **1a** was optimized by DFT calculations using the Gaussian 03 program at the B3LYP level of theory and 6-31G (d,p) basis set. Autodock Tools was used to generate the pdbqt files required for both the DNA and the complex. All the polar hydrogens were added, and non-polar hydrogens emerged from the structure. The DNA structure was kept rigid during the docking while the ligand was allowed to have rotatable bonds. The DNA motif was enclosed in the grid box defined by Auto Grid (dimensions 40" \times 40" \times 40" Å) used for dispersion/repulsion, hydrogen bonding, electrostatics, and desolvation. Auto Grid performed a pre-calculated atomic affinity grid map for each atom type in the ligand plus an electrostatic map and a separate desolvation map for the substrate molecule. Then, during the AutoDock calculation, the energetics of a particular ligand configuration was evaluated using the values from the grids. Ligand docking was carried out with the AutoDock 4.2 Lamarckian Genetic Algorithm (LGA) with an initial population of 150 randomly placed individuals, a maximum number of 25×10^6 energy evaluations, and a probability of performing local search on individual of 0.15. The results of 150 independent docking runs were clustered with a RMSD of 5.0 Å. Other parameters were set

as default. The selected docking solution was the most energetically favourable from the most populated cluster. The most stabilized nucleoside-DNA complex structure was imaged using Chimera 1.11.2 software.

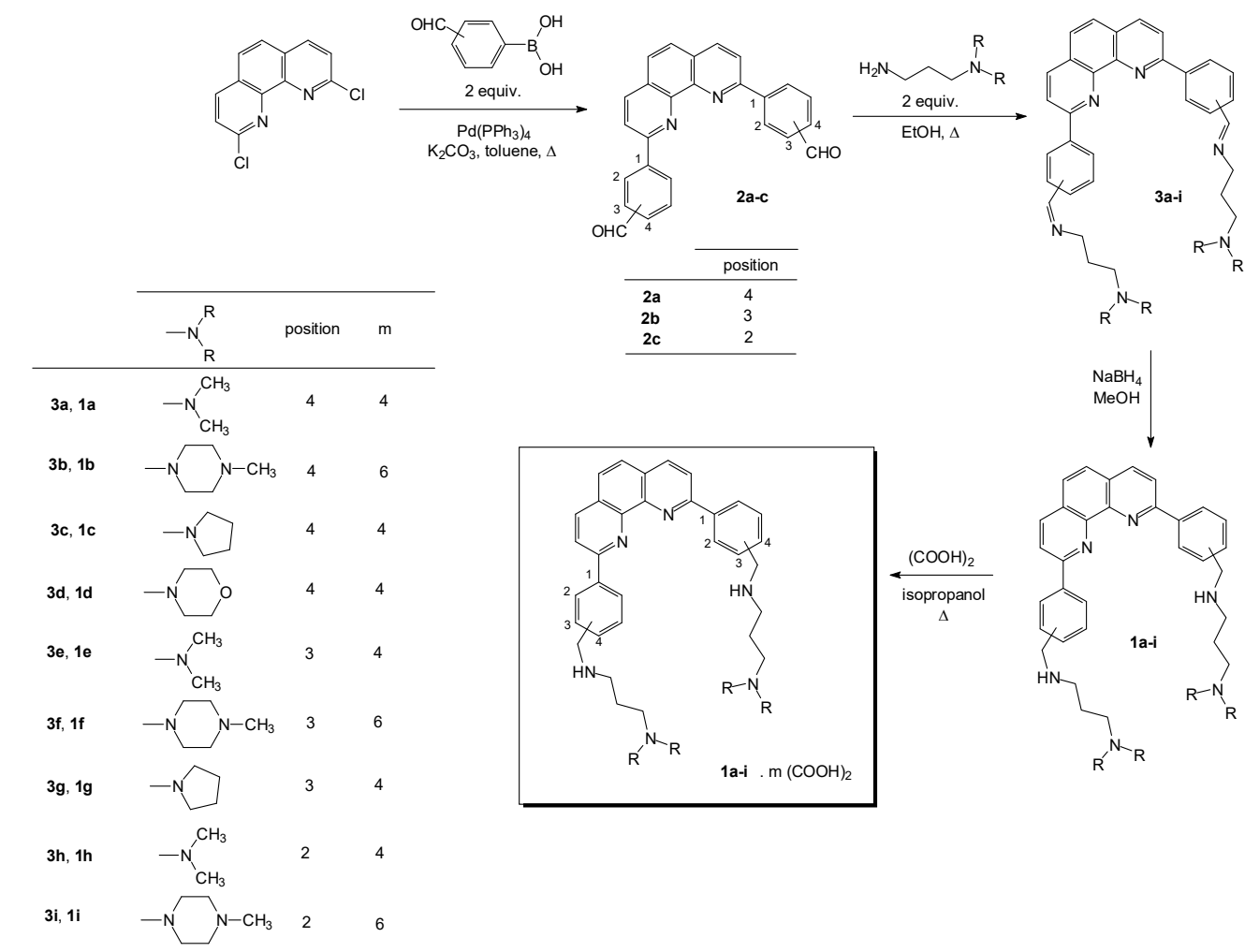
Acknowledgments: We thank Dr. Jean-Baptiste Boulé for providing Pif1 helicase, the IECB BPCS technical platform and the Aquitaine Regional Council and Agence Nationale de la Recherche [ANR Quarpdiem, ANR-12-BSV8-0008-01 to J.L.M.] for funding.

References

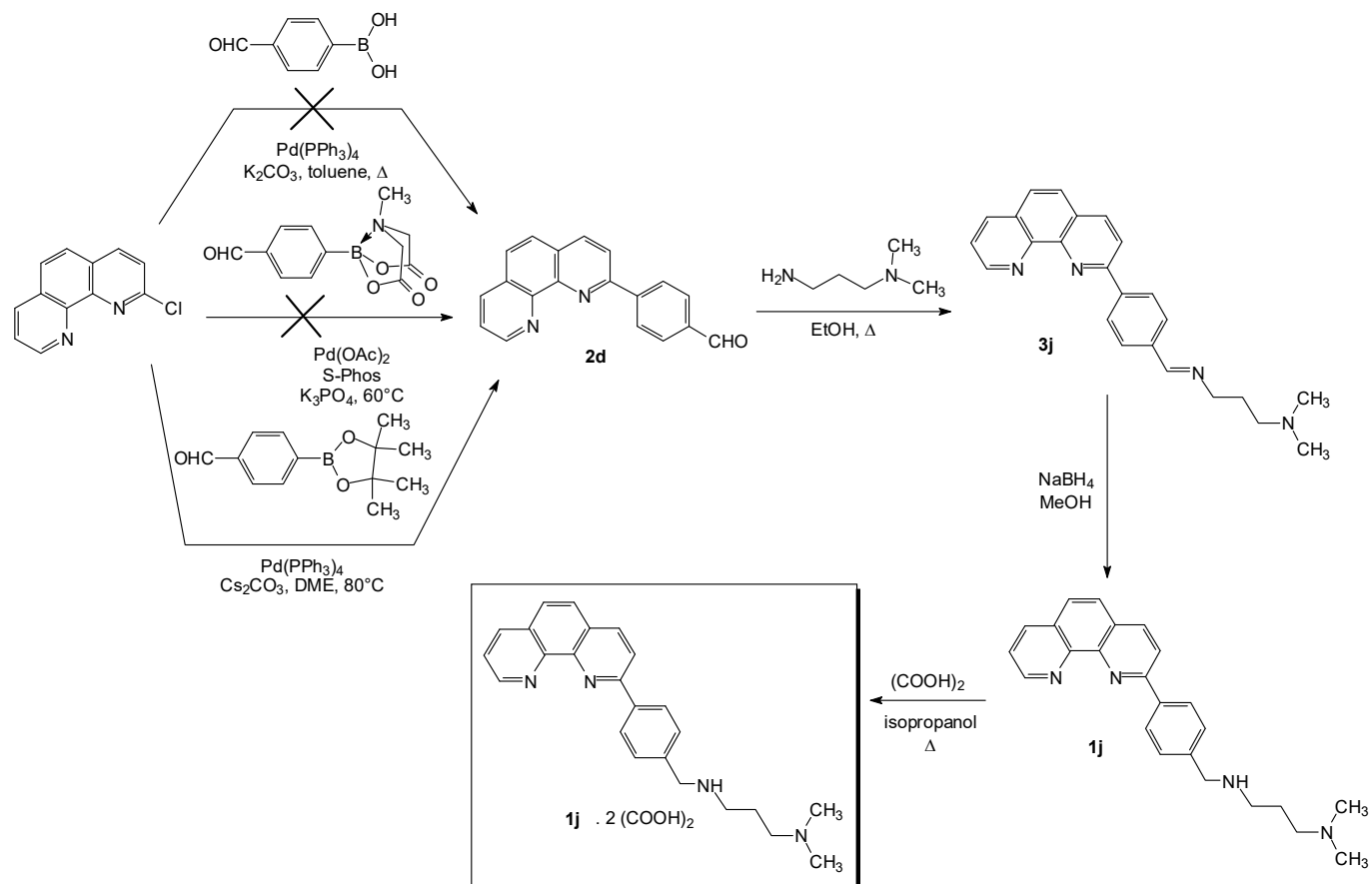
- [1] P. Bates, J.-L. Mergny, D. Yang, *EMBO Rep.* **2007**, *8*, 1003–1010.
- [2] G. Biffi, D. Tannahill, M. John, S. Balasubramanian, *Nat. Chem.* **2013**, *5*, 182–186.
- [3] A. Henderson, Y. Wu, Y. C. Huang, E. a. Chavez, J. Platt, F. B. Johnson, R. M. Brosh, D. Sen, P. M. Lansdorp, *Nucleic Acids Res.* **2014**, *42*, 860–869.
- [4] S. G. Hershman, Q. Chen, J. Y. Lee, M. L. Kozak, P. Yue, L. S. Wang, F. B. Johnson, *Nucleic Acids Res.* **2008**, *36*, 144–156.
- [5] J. L. Huppert, S. Balasubramanian, *Nucleic Acids Res.* **2005**, *33*, 2908–2916.
- [6] A. Bedrat, L. Lacroix, J.-L. Mergny, *Nucleic Acids Res.* **2016**, *44*, 1746–59.
- [7] V. S. Chambers, G. Marsico, J. M. Boutell, M. Di Antonio, G. P. Smith, S. Balasubramanian, *Nat. Biotechnol.* **2015**, *33*, 877–881.
- [8] D. Rhodes, H. J. Lipps, *Nucleic Acids Res.* **2015**, *43*, gkv862.
- [9] H. J. Lipps, D. Rhodes, *Trends Cell Biol.* **2009**, *19*, 414–22.
- [10] V. Brázda, L. Hároníková, J. Liao, M. Fojta, *Int. J. Mol. Sci.* **2014**, *15*, 17493–17517.
- [11] N. Maizels, *EMBO Rep.* **2015**, *16*, 910–922.
- [12] J. Eddy, N. Maizels, *Nucleic Acids Res.* **2006**, *34*, 3887–3896.
- [13] Q. Wang, J. Liu, Z. Chen, K. Zheng, C. Chen, Y.-H. Hao, Z. Tan, *Nucleic Acids Res.* **2011**, *39*, 6229–37.
- [14] S. Neidle, *FEBS J.* **2010**, *277*, 1118–1125.
- [15] J. Bidzinska, G. Cimino-Reale, N. Zaffaroni, M. Folini, *Molecules* **2013**, *18*, 12368–12395.
- [16] S. Neidle, *J. Med. Chem.* **2016**, acs.jmedchem.5b01835.
- [17] A. De Cian, E. DeLemos, J. L. Mergny, M. P. Teulade-Fichou, D. Monchaud, *J. Am. Chem. Soc.* **2007**, *129*, 1856–1857.
- [18] H. Li, C. Wei, *Bioorg. Med. Chem. Lett.* **2015**, *25*, 3798–3803.
- [19] M. C. Nielsen, J. Borch, T. Ulven, *Bioorg. Med. Chem.* **2009**, *17*, 8241–8246.
- [20] C. Musetti, L. Lucatello, S. Bianco, a. P. Krapcho, S. A. Cadamuro, M. Palumbo, C. Sissi, *Dalt. Trans.* **2009**, 3657.
- [21] M. C. Nielsen, A. F. Larsen, F. H. Abdikadir, T. Ulven, *Eur. J. Med. Chem.* **2014**, *72*, 119–26.
- [22] A. F. Larsen, T. Ulven, *Org. Lett.* **2011**, *13*, 3546–3548.
- [23] A. F. Larsen, M. C. Nielsen, T. Ulven, *Chem. - A Eur. J.* **2012**, *18*, 10892–10902.
- [24] J. Amato, N. Iaccarino, B. Pagano, R. Morigi, A. Locatelli, A. Leoni, M. Rambaldi, P. Zizza, A. Biroccio, E. Novellino, et al., *Front. Chem.* **2014**, *2*, 54.
- [25] L. Wang, Y. Wen, J. Liu, J. Zhou, C. Li, C. Wei, *Org. Biomol. Chem.* **2011**, *9*, 2648–53.
- [26] L. Wang, C. Wei, *Chem. Biodivers.* **2013**, *10*, 1154–64.
- [27] S. Liao, Z. Zhang, Q. Wu, X. Wang, W. Mei, *Bioorg. Med. Chem.* **2014**, *22*, 6503–8.
- [28] H. Zhang, J. Xiang, H. Hu, Y. Liu, F. Yang, G. Shen, Y. Tang, C. Chen, *Int. J. Biol. Macromol.* **2015**, *78*, 149–156.
- [29] S. a Ohnmacht, S. Neidle, *Bioorg. Med. Chem. Lett.* **2014**, *24*, 2602–12.
- [30] M. Beyler, V. Heitz, J.-P. Sauvage, *J. Am. Chem. Soc.* **2010**, *132*, 4409–17.
- [31] M. Linke, J. C. Chambron, V. Heitz, J. P. Sauvage, S. Encinas, F. Barigelletti, L. Flamigni, *J. Am. Chem. Soc.* **2000**, *122*, 11834–11844.
- [32] K. Yasukawa, R. Maeda, H. Tokailin, *Phenanthroline Compounds, Electron Transport Material Obtained from Said Compound, and Organic Thin-Film Photovoltaic Cell Comprising Said Compound*, **2013**, EP 2599780 A1.
- [33] Y. Wang, D. J. Patel, *Structure* **1993**, *1*, 263–82.
- [34] Y. Xu, Y. Noguchi, H. Sugiyama, *Bioorganic Med. Chem.* **2006**, *14*, 5584–5591.
- [35] D. Renciuik, I. Kejnovská, P. Skoláková, K. Bednářová, J. Motlová, M. Vorlícková, *Nucleic Acids Res.* **2009**, *37*, 6625–34.
- [36] J. Dai, M. Carver, C. Punchihewa, R. a. Jones, D. Yang, *Nucleic Acids Res.* **2007**, *35*, 4927–4940.
- [37] a. T. Phan, *FEBS J.* **2010**, *277*, 1107–1117.
- [38] F. Hamon, E. Largy, A. Guédin-Beaurepaire, M. Rouchon-Dagois, A. Sidibe, D. Monchaud, J. L. Mergny, J. F. Riou, C. H. Nguyen, M. P. Teulade-Fichou, *Angew. Chemie - Int. Ed.* **2011**, *50*, 8745–8749.
- [39] J. M. Nicoludis, S. P. Barrett, J. L. Mergny, L. a. Yatsunyk, *Nucleic Acids Res.* **2012**, *40*, 5432–5447.
- [40] A. De Rache, J.-L. Mergny, *Biochimie* **2015**, *115*, 194–202.
- [41] S. Amrane, M. Adrian, B. Heddi, A. Serero, A. Nicolas, J. Mergny, A. Tua, *J. Am. Chem. Soc.* **2012**, *134*, 5807–5816.
- [42] Ambrus Attila, C. Ding, D. Jixun, J. R. A, D. Yang, *Biochemistry* **2005**, 2048–2058.
- [43] R. F. Macaya, P. Schultze, F. W. Smith, J. A. Roe, J. Feigon, *Proc. Natl. Acad. Sci. U. S. A.* **1993**, *90*, 3745–9.
- [44] S. Amrane, R. W. L. Ang, Z. M. Tan, C. Li, J. K. C. Lim, J. M. W. Lim, K. W. Lim, A. T. Phan, *Nucleic Acids Res.* **2009**, *37*, 931–938.
- [45] K. W. Lim, P. Alberti, A. Guédin, L. Lacroix, J. F. Riou, N. J. Royle, J. L. Mergny, A. T. Phan, *Nucleic Acids Res.* **2009**, *37*, 6239–6248.
- [46] L. Lecarme, E. Prado, A. De Rache, M.-L. Nicolau-Travers, R. Bonnet, A. van Der Heyden, C. Philouze, D. Gomez, J.-L. Mergny, H. Jamet, et al., *Inorg. Chem.* **2014**, *53*, 12519–31.
- [47] A. Marchand, A. Granzhan, K. Iida, Y. Tsushima, Y. Ma, K. Nagasawa, M.-P. Teulade-Fichou, V. Gabelica, J.

- Am. Chem. Soc.* **2015**, *137*, 750–756.
- [48] M. Bončina, Č. Podlipnik, I. Piantanida, J. Eilmes, M.-P. Teulade-Fichou, G. Vesnaver, J. Lah, *Nucleic Acids Res.* **2015**, *43*, 10376–86.
- [49] A. Marchand, V. Gabelica, *J. Am. Soc. Mass Spectrom.* **2014**, *25*, 1146–1154.
- [50] G. N. Parkinson, M. P. H. Lee, S. Neidle, *Nature* **2002**, *417*, 876–880.
- [51] C. Ribeyre, J. Lopes, J.-B. Boulé, A. Piazza, A. Guédin, V. a Zakian, J.-L. Mergny, A. Nicolas, *PLoS Genet.* **2009**, *5*, e1000475.
- [52] K. Paeschke, J. a Capra, V. a Zakian, *Cell* **2011**, *145*, 678–91.
- [53] J.-B. Boulé, L. R. Vega, V. A. Zakian, *Nature* **2005**, *438*, 57–61.
- [54] O. Mendoza, N. M. Gueddouda, J.-B. Boule, A. Bourdoncle, J.-L. Mergny, *Nucleic Acids Res.* **2015**, *43*, e71–e71.
- [55] D. R. Tobergte, S. Curtis, in *Clim. Chang. 2013 - Phys. Sci. Basis* (Ed.: Intergovernmental Panel on Climate Change), Cambridge University Press, Cambridge, **2013**, pp. 1–30.
- [56] G. M. Sheldrick, *Acta Crystallogr. Sect. A Found. Crystallogr.* **2007**, *64*, 112–122.
- [57] A. De Cian, L. Guittat, M. Kaiser, B. Saccà, S. Amrane, A. Bourdoncle, P. Alberti, M.-P. Teulade-Fichou, L. Lacroix, J.-L. Mergny, *Methods* **2007**, *42*, 183–95.
- [58] A. De Rache, N.M. Gueddouda, A. Bourdoncle, P. Hommes, H.U. Reißig, J.-L. Mergny, *Chemistry* **2016**, *22*, 12651-12654.
- [59] K. W. Lim, P. Alberti, A. Guédin, L. Lacroix, J.-F. Riou, N. J. Royle, J.-L. Mergny, A. T. Phan, *Nucl. Acids Res.*, **2009**, *37*, 6239-6248.
- [60] K.N. Luu, A.T. Phan, V.V. Kuryavyi, L. Lacroix, D.J. Patel, *J. Am. Chem. Soc.* **2006**, *128*, 9963-9970.

Figures



Scheme 1. Synthesis of 2,9-bis[(substituted-aminomethyl)phenyl]-1,10-phenanthrolines **1a-i**.



Scheme 2. Synthesis of 2-{4-[(3-dimethylaminopropyl)aminomethyl]phenyl}-1,10-phenanthroline **1j**.

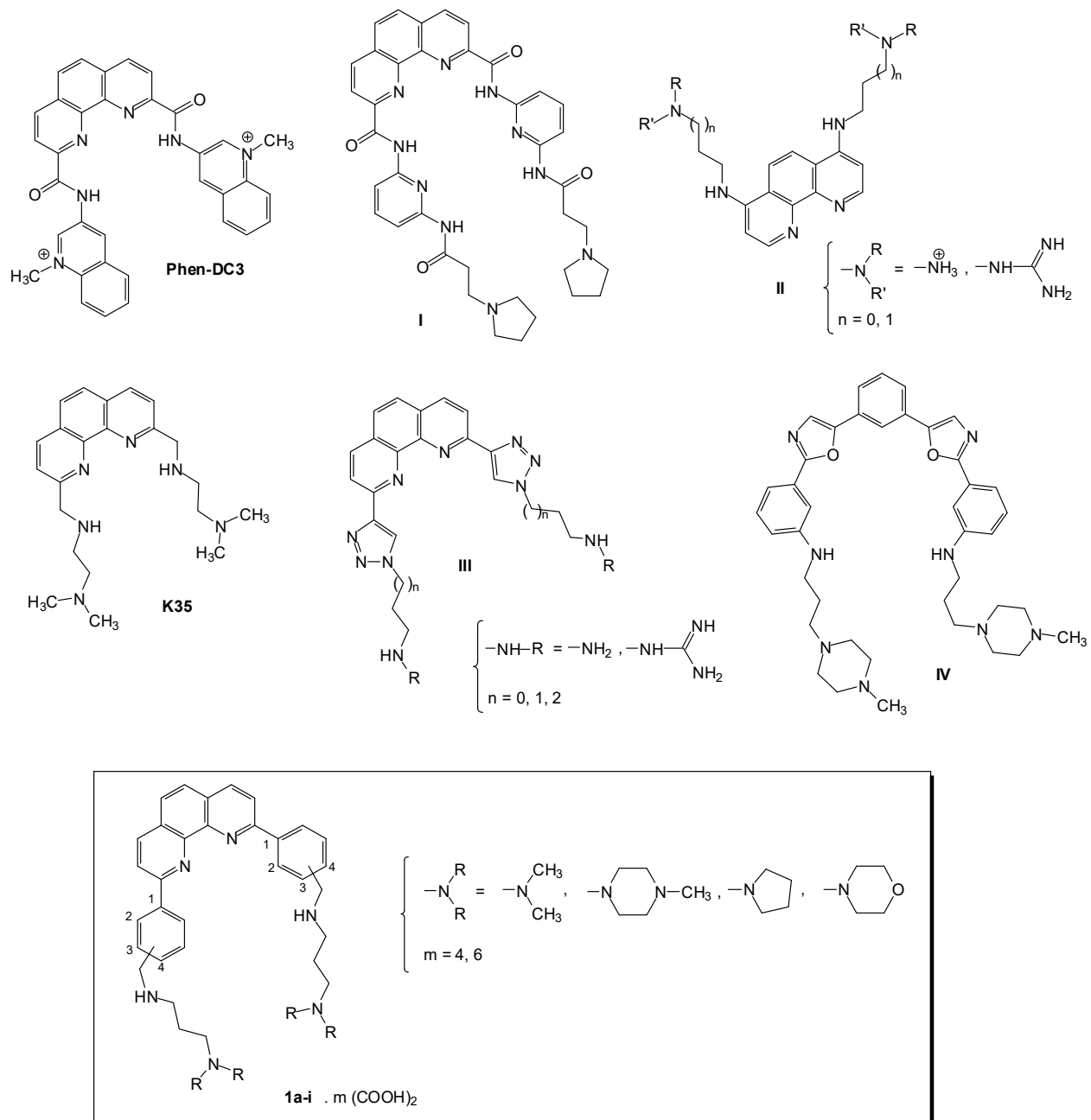


Figure 1. Structures of **Phen-DC3**, phenanthroline derivatives **I-III**, **K35**, disubstituted phenyl bis-oxazole **IV** and 2,9-bis[(substituted-aminomethyl)phenyl]-1,10-phenanthroline derivatives **1a-i**.

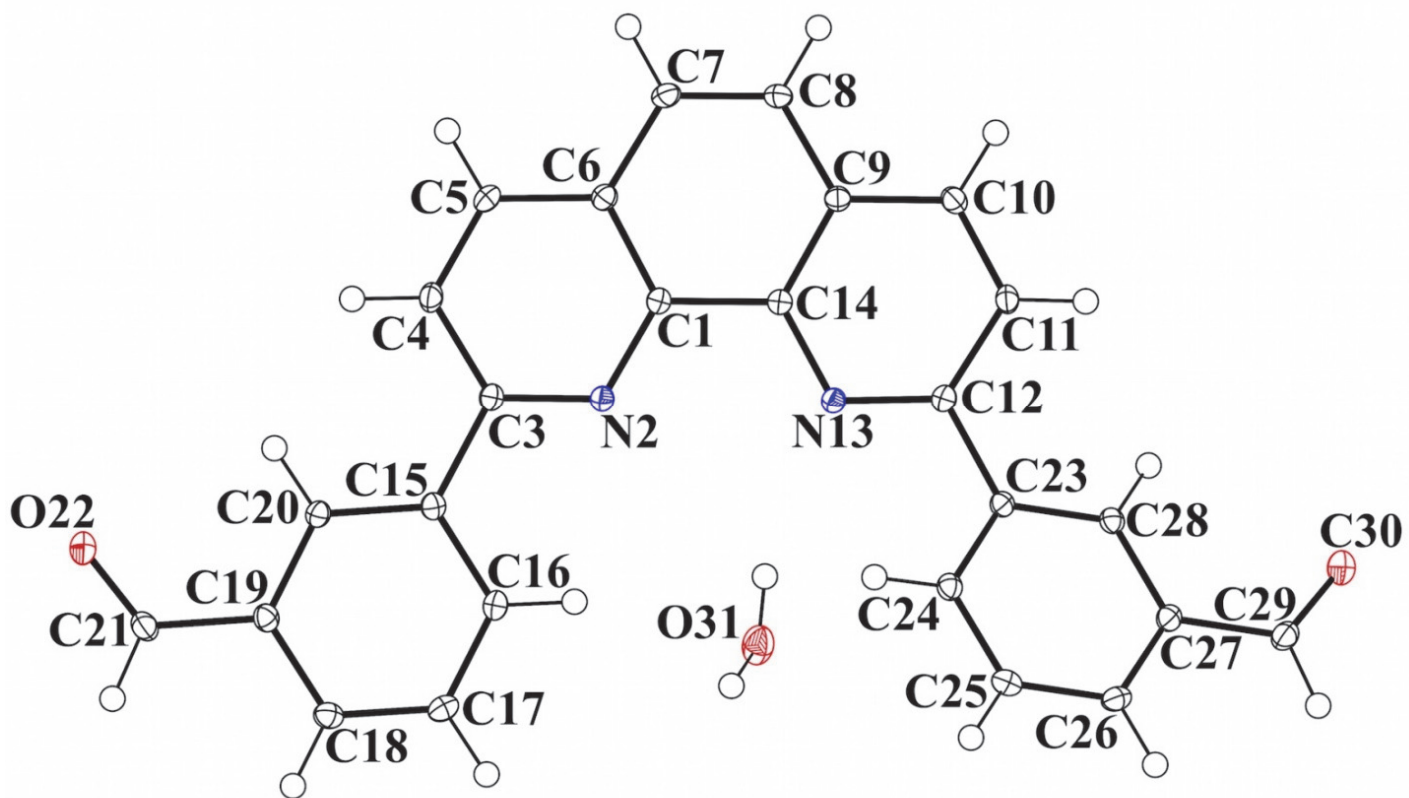


Figure 2. The ORTEP drawing of bis-[2,9-(3-formylphenyl)]-1,10-phenanthroline **2b** with thermal ellipsoids at 30% level.

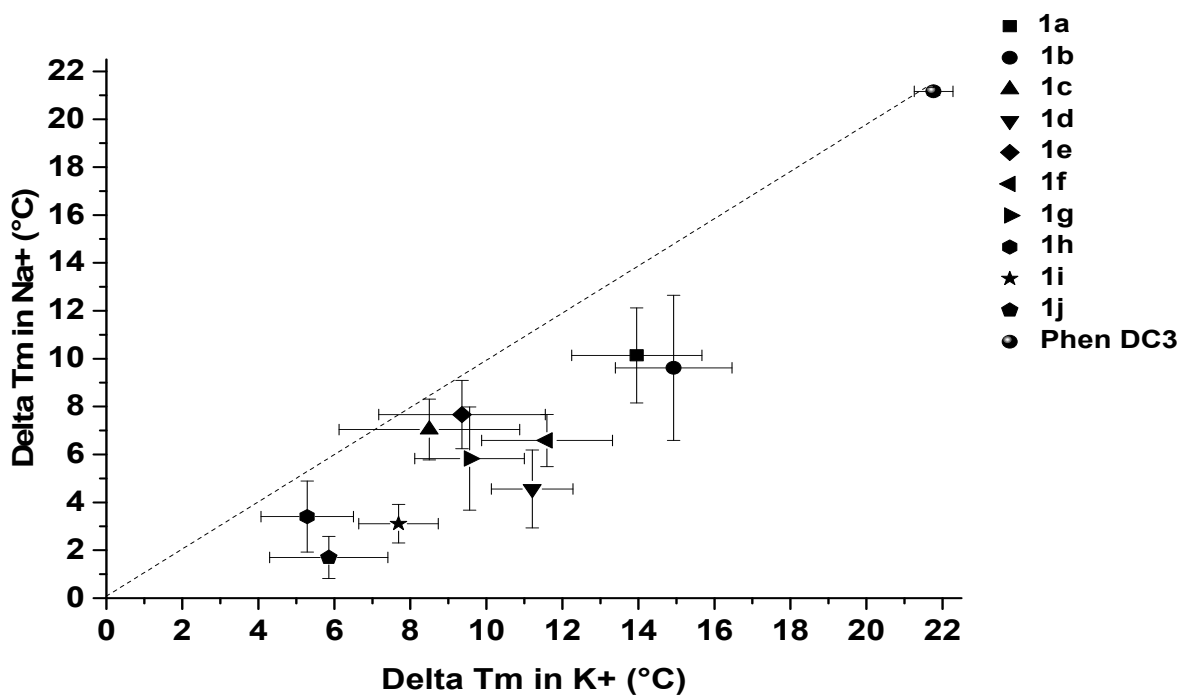


Figure 3. Stabilization of F21T (0.2 μM) by compounds **1a-j** (1 μM). Comparison of $\Delta T_{(1/2)}$ in K^+ conditions vs. $\Delta T_{(1/2)}$ in Na^+ conditions. Dashed line represents an equal stabilization in K^+ and Na^+ conditions. In K^+ , the $T_{(1/2)}$ in the absence of ligand is 52.2 ± 0.8 $^{\circ}\text{C}$ and that in Na^+ is 49.4 ± 1.0 $^{\circ}\text{C}$

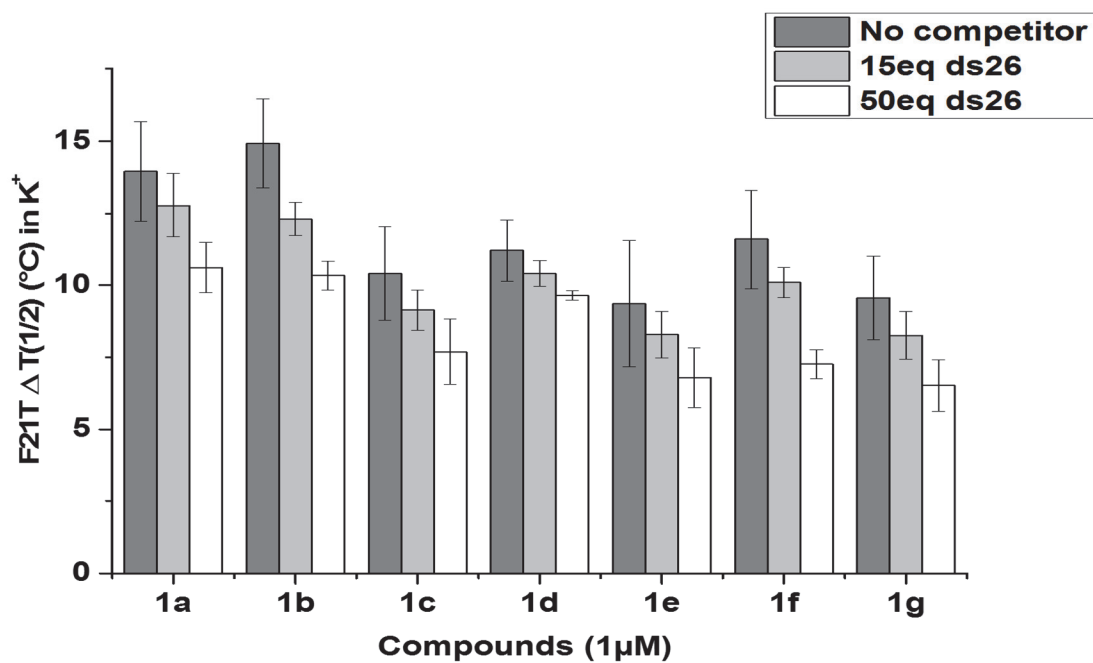


Figure 4. Stabilization of F21T (0.2 μM) by **1a-g** (1 μM) in the presence of ds26. Comparison of $\Delta T_{1/2}$ in K^+ conditions in absence of competitor vs. $\Delta T_{(1/2)}$ in K^+ conditions in presence of competitor ds26. Dark grey bars represent the F21T $\Delta T_{1/2}$ with 1 μM ligand, light grey bars represent F21T $\Delta T_{1/2}$ in presence of with 1 μM ligand and 15 eq of ds26, and white bars represent F21T $\Delta T_{1/2}$ in presence of with 1 μM ligand and 50 eq excess of ds26.

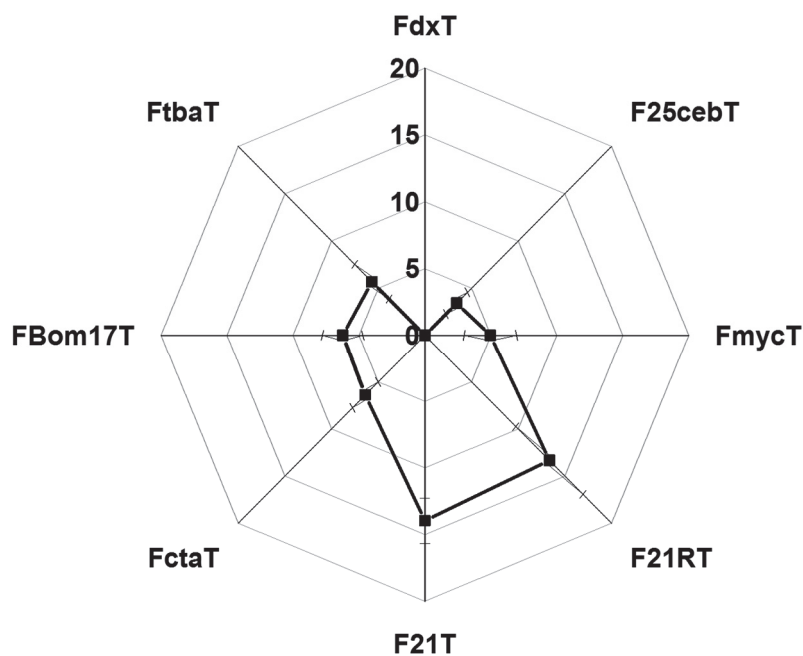


Figure 5. Stabilization specificity profile of **1a** (1 μM) toward a chosen panel of oligonucleotides that adopt different conformations. The difference in $T_{1/2}$ with and without 0.2 μM **1a**, $\Delta T_{1/2}$, in $^{\circ}\text{C}$ is plotted. Experiments were performed in 10 mM lithium cacodylate buffer (pH 7.2), 90 mM LiCl, and 10 mM KCl. FdxT is a duplex ($T_{1/2}$ without ligand = 67.6 ± 0.3 $^{\circ}\text{C}$), F25cebT ($T_{1/2} = 69.3 \pm 0.4$ $^{\circ}\text{C}$) and FmycT ($T_{1/2} = 66.3 \pm 0.9$ $^{\circ}\text{C}$) adopt parallel G4 conformations. FctaT ($T_{1/2} = 58.8 \pm 0.2$ $^{\circ}\text{C}$), FBom17T ($T_{1/2} = 49.7 \pm 0.8$ $^{\circ}\text{C}$) and FtbaT ($T_{1/2} = 52.9 \pm 0.7$ $^{\circ}\text{C}$) adopt antiparallel conformations. F21T ($T_{1/2} = 52.2 \pm 0.8$ $^{\circ}\text{C}$) adopts a mix of antiparallel and hybrid conformations. The RNA F21RT ($T_{1/2} = 56.2 \pm 0.7$ $^{\circ}\text{C}$) was assessed in 10 mM lithium cacodylate buffer (pH 7.2), 99 mM LiCl, and 1 mM KCl; it adopts a parallel conformation.

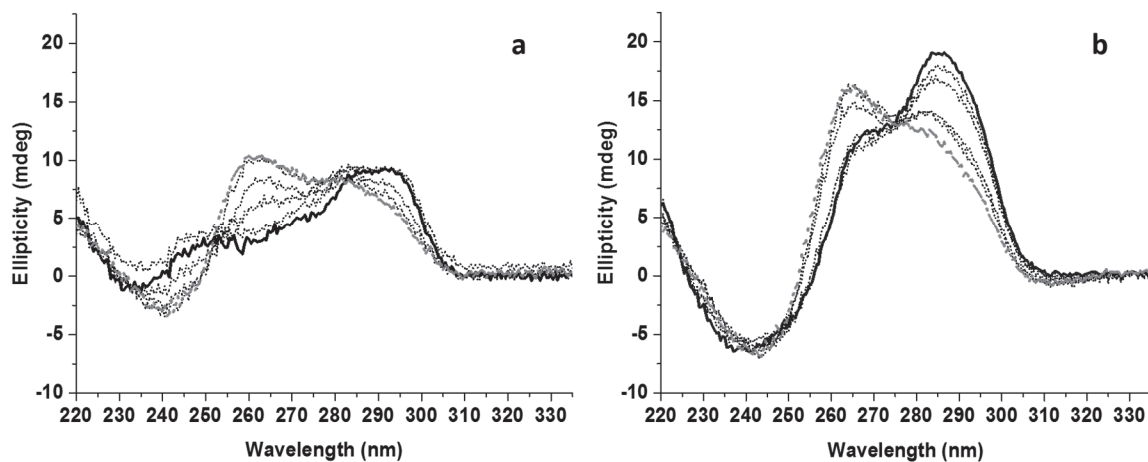


Figure 6. CD titration of (a) 22AG (3 μ M) and (b) 24TTG (3 μ M) with **1a**. CD spectra were recorded in 10 mM lithium cacodylate buffer (pH 7.3), 90 mM LiCl, and 10 mM KCl. Solid lines correspond to the CD profile in the absence of **1a**, dotted black lines correspond to the spectra after sequential additions of 4 equivalents of **1a** one equivalent at a time, and grey dotted lines correspond to the CD profile in the presence of 5 equivalents of **1a**.

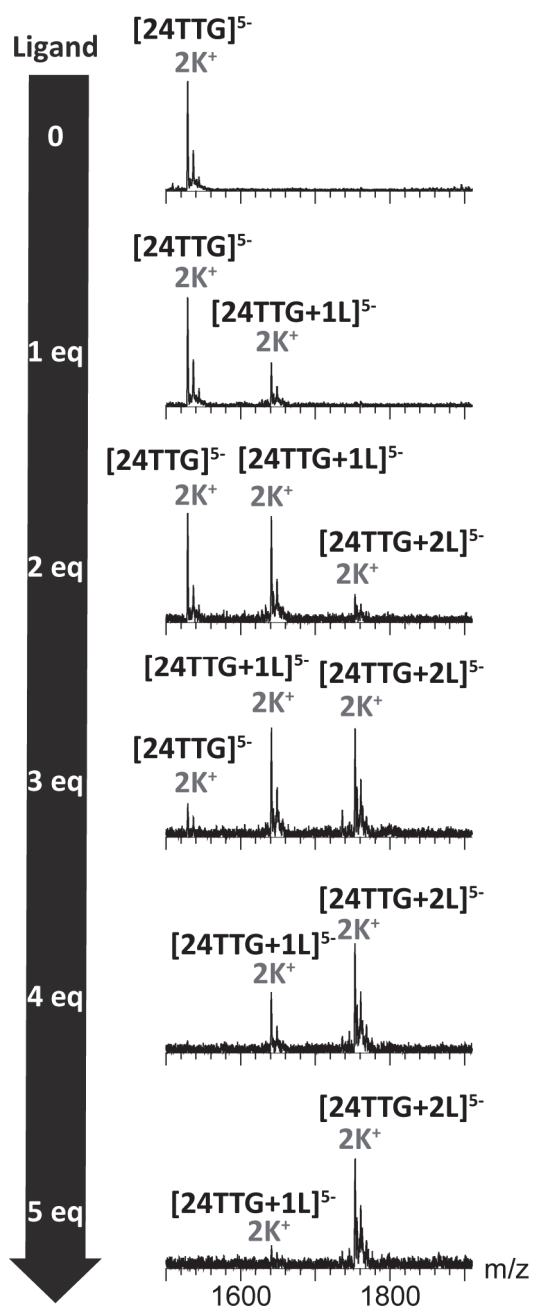


Figure 7. Electrospray mass spectrometry titration of 24TTG (10 μ M) with ligand **1a**. All spectra were recorded in 100 mM TMAA and 1 mM KCl in presence of the indicated amount of **1a** (from 0 to 5 equivalents as compared to the DNA concentration).

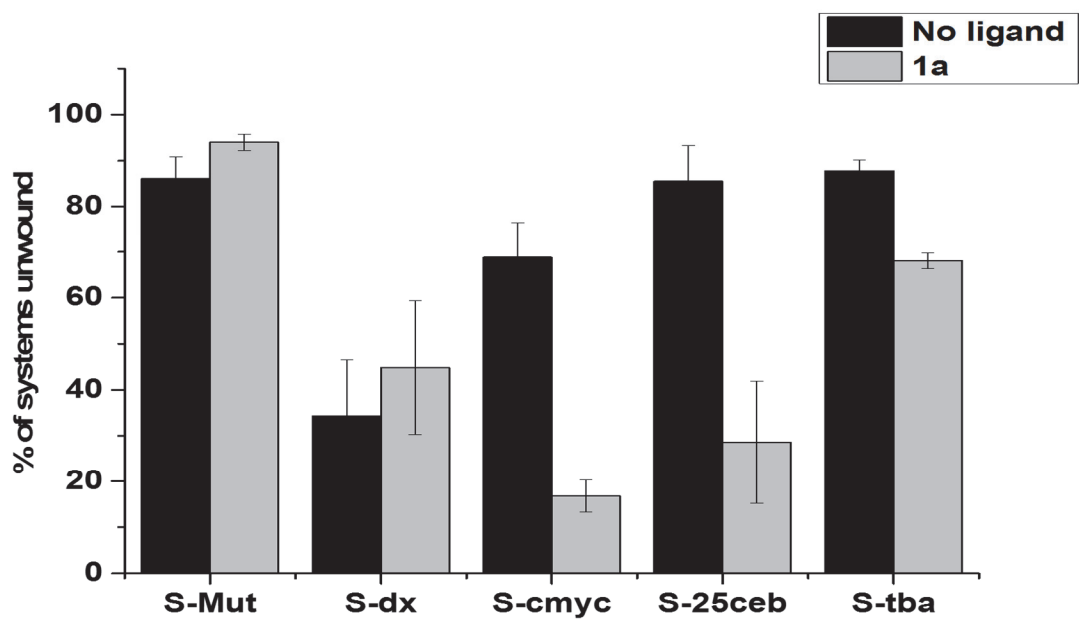


Figure 8. Fluorescence-based helicase assay with **1a** and substrates containing indicated control (S-Mut and S-dx) or G4-forming regions from cmyc, ced, and tba. Black: without **1a**, grey: with **1a**.

Table 1. Physical properties of **1a-j** oxalates.

Compound		Salt ^[a]	mp (°C) ^[b]	% Yield ^[c]
1a	Beige crystals	4 (COOH) ₂	202	87
1b	Beige crystals	6 (COOH) ₂	> 240	78
1c	Yellow crystals	4 (COOH) ₂	197	79
1d	Pale-yellow crystals	4 (COOH) ₂	> 240	62
1e	Pale-orange crystals	4 (COOH) ₂	232	62
1f	Pale-yellow crystals	6 (COOH) ₂	220	76
1g	Beige crystals	4 (COOH) ₂	171	82
1h	Beige crystals	4 (COOH) ₂	96	74
1i	Beige crystals	6 (COOH) ₂	168	80
1j	Pale-orange crystals	2 (COOH) ₂	141	88

^[a]The stoichiometries and compositions of the salts were determined by elemental analyses (within ±0.4% of the theoretical values).

^[b]Crystallization solvent: 2-PrOH–H₂O.

^[c]The yields only include the conversions into the ammonium oxalates.

Table 2. FRET-melting values for **PhenDC3** and compounds **1a-j** with F21T in K⁺ conditions.

Compound	F21T $\Delta T_{(1/2)}$ °C ^[a]	Selectivity index ^[b]
PhenDC3	21.8±0.5	0.99±0.0
1a	14±1.7	0.92±0.2
1b	14.9±1.5	0.82±0.1
1c	10.4±1.6	0.88±0.2
1d	11.2±1.1	0.93±0.1
1e	9.4±2.2	0.89±0.3
1f	11.6±1.7	0.87±0.2
1g	9.6±1.4	0.86±0.2
1h	5.3±1.2	nd ^[c]
1i	7.7±1.0	nd
1j	5.9±1.6	nd

^[a] $\Delta T_{1/2}$ (°C) of F21T (0.2 μ M) is reported at 1 μ M ligand concentration in 10 mM lithium cacodylate (pH 7.2), 10 mM KCl and 90 mM LiCl. **PhenDC3** was used as control compound. F21T $\Delta T_{1/2}$ in K⁺ = 52.2 ± 0.8 °C.

^[b]Selectivity index in K⁺ conditions for 1 μ M of each compound was based on the ratio between F21T $\Delta T_{1/2}$ in presence of 3 μ M of ds26 and F21T $\Delta T_{1/2}$ in absence of competitor.

^[c]nd= not determined for compounds exhibiting a low (<10 °C) stabilisation at 1 μ M ligand concentration in K⁺ conditions.